



HAL
open science

Structural diagenesis of shallow platform carbonates: Role of early embrittlement on fracture setting and distribution, case study of Monte Alpi (Southern Apennines, Italy)

Vincenzo La Bruna, Juliette Lamarche, Fabrizio Agosta, Andrea Rustichelli,
Alessandro Giuffrida, Roland Salardon, Lionel Marié

► To cite this version:

Vincenzo La Bruna, Juliette Lamarche, Fabrizio Agosta, Andrea Rustichelli, Alessandro Giuffrida, et al.. Structural diagenesis of shallow platform carbonates: Role of early embrittlement on fracture setting and distribution, case study of Monte Alpi (Southern Apennines, Italy). *Journal of Structural Geology*, 2020, 131, pp.103940. 10.1016/j.jsg.2019.103940 . hal-03164540

HAL Id: hal-03164540

<https://hal.science/hal-03164540v1>

Submitted on 25 Nov 2022

HAL is a multi-disciplinary open access archive for the deposit and dissemination of scientific research documents, whether they are published or not. The documents may come from teaching and research institutions in France or abroad, or from public or private research centers.

L'archive ouverte pluridisciplinaire **HAL**, est destinée au dépôt et à la diffusion de documents scientifiques de niveau recherche, publiés ou non, émanant des établissements d'enseignement et de recherche français ou étrangers, des laboratoires publics ou privés.



Distributed under a Creative Commons Attribution - NonCommercial 4.0 International License

1 Structural diagenesis of shallow platform carbonates: role of early embrittlement on fracture
2 setting and distribution, case study of Monte Alpi (Southern Apennines, Italy)

3
4 Vincenzo La Bruna^{a, b, 1}, Juliette Lamarche^a, Fabrizio Agosta^{c, 1}, Andrea Rustichelli^{d, 1}, Alessandro Giuffrida^{c, 1},
5 Roland Salardon^b, Lionel Marié^b

6
7 ^a*Aix Marseille Univ, CNRS, IRD, INRA, Coll France, CEREGE, Aix-en-Provence, France*

8 ^b*Federal University of Rio Grande do Norte, Natal, Brazil*

9 ^c*Department of Science, University of Basilicata, Italy*

10 ^d*School of Science and Technology, University of Camerino, Italy*

11 ¹Reservoir Characterization Project (www.rechproject.com).

12
13 **Abstract**

14 Bed-perpendicular, opening-mode diffuse fractures are common features in carbonate rocks because
15 they become brittle during the first stages of diagenesis. Early- fractures could be independent of
16 tectonics and form a background structural network from sub-millimeter to 10's of centimetres scale.
17 This study focuses on the outcrop-to-micro scales structural, stratigraphic, and petrographic
18 characterization of Lower Cretaceous, shallow-water, tight limestones of the Inner Apulian Platform
19 exposed along the axial sector of the southern Apennines fold-and-thrust belt, Italy. This work aims at
20 understanding the formation of early diagenetic fractures during the first stages of sediment
21 lithification, and on their impact on subsequent deformation mechanisms associated to polyphase
22 tectonics. The results of field structural surveys, of petrographic and cathodoluminescence analyses of
23 representative samples unravel the main structural-diagenetic processes in shallow-water carbonates.
24 We document that early brittle fractures were intrinsically related to the host rock pore type and
25 cementation processes, and summarize the overall time-dependant evolution of the structural
26 assemblages in a conceptual model. This model includes all abutting and crosscutting relationships
27 among the various structural elements from field to thin-section observation, and form the now days
28 fracture network.

29

30 Keywords: Fractures; Carbonates; Early cementation; Diagenesis; Reservoirs; Southern Apennines;

31

32 **1. Introduction**

33 Carbonate reservoirs are of a great importance for hydrocarbon exploitation, water resource, and gas
34 sequestration (Barlét-Gouédard et al., 2006; Ford and Williams, 2007; Ahr, 2011). These reservoirs are
35 very often characterized by both primary and secondary heterogeneities (Nelson, 2001; Lucia, 2007),
36 which occur from regional (100's of m to km), to outcrop (cm to 100 m) and micro-scale (mm to cm).
37 In reservoir modelling, heterogeneities with dimensional properties smaller than 10m are included
38 into the matrix properties, leading to quite unrealistic scenarios in the case of fractured carbonates,
39 which have been subjected to complex diagenetic and tectonic histories (Warren and Root, 1963;
40 Barbier et al., 2012; Matonti et al., 2015; Giorgioni et al., 2016; Panza et al., 2016; Giuffrida et al.,
41 2019a). Particularly in tight carbonates, both outcrop-scale and micro-scale fractures may drive a
42 large amount of geofluids (Guerriero et al., 2013; Anders et al., 2014; Panza et al., 2019). Since cement-
43 bearing fractures are widespread in the subsurface, fluid can only flow where fractures are now days
44 barren or partly cemented (Aguilera, 1998; Nelson, 2001; Laubach, 2003; Matonti et al., 2017). Hence,
45 deciphering the interaction between fractures and diagenesis is a key point for a good understanding
46 of the reservoir properties. Accordingly, the assessment of fracture timing and sealing due to
47 cementation is of a prime importance for fractured carbonate reservoir analysis (Laubach et al., 2010;
48 Vitale et al., 2012). In the last decade, the few studies that focused on the relationships between
49 structural and diagenetic processes in carbonates pointed out the possible occurrence of a early
50 embrittlement (Frost and Kerans, 2010; Lavenu et al., 2013, 2014; Lamarche 2015a; Lamarche et al.,
51 2015b; Tavani et al., 2016; Vinci et al., 2017; Lavenu and Lamarche 2018). Along this line, the analysis
52 of outcrop analogues of subsurface fractured carbonates is often employed to lower the uncertainties
53 and bias associated to reservoir characterization and modelling (Lamarche et al., 2012; Rustichelli et
54 al., 2013; Agosta et al., 2015; Lavenu et al., 2015; Corradetti et al., 2018; Guerriero et al., 2015; Panza et
55 al., 2016, 2018, 2019; Massaro et al., 2018; Giuffrida et al., 2019a). In this paper, we investigate the
56 polyphase diagenetic history of fractures crosscutting shallow-water platform carbonates of Monte

57 Alpi, southern Italy (Sartoni and Crescenti, 1962; Corrado et al. 2002; Shiner et al., 2004; Mazzoli et al.,
58 2006, 2008; La Bruna et al., 2017, 2018). This massif can be considered as a good structural analogue
59 for nearby oil fields of the Basilicata Region, as well as a case study for a multi-scale analysis of
60 carbonate reservoirs involved in a complex tectonic history. In light of their time-dependant tectonic
61 evolution, the goal of the present work is to assess the control exerted by carbonate facies on the
62 structural diagenesis of the Lower Cretaceous limestones.

63

64 **2. Geological setting**

65 The Apennines are an arc-shaped fold-and-thrust belt (FTB) due to the Oligocene-to-Pleistocene
66 continental collision between Eurasian and African plates (Patacca and Scandone, 2007, and
67 references therein). Contractual deformation was characterized by the eastward propagation of
68 thrust sheets, which involved Meso-Cenozoic sedimentary successions originally pertaining to the
69 Neo-Tethys Ocean due to the rollback of the Adriatic slab (Royden et al., 1987; Patacca et al., 1990;
70 Doglioni, 1991). Along-strike, the Apennines are divided into northern, central, and southern sectors
71 which are bounded by lithospheric discontinuities trending almost orthogonal to the belt axis
72 (Locardi, 1988; Ghisetti and Vezzani, 1997; Vai and Martini, 2001; Cavazza et al., 2004). From west to
73 east, the now days tectono-stratigraphic units comprising the southern Apennines FTB are (Patacca
74 and Scandone, 2007): (i) siltstones and claystones of the Liguride/Sicilide oceanic Basin; ii) carbonates
75 derived from the Apennine Platform; iii) mixed terrigenous-carbonate rocks derived from the
76 Lagonegro Basin, which are commonly divided into Lagonegro I and II tectonic units; and iv)
77 carbonates of the Apulian Platform (Fig. 1). During Late Pliocene-Early Pleistocene time, the western
78 and inner portion of the Apulian Platform (Mostardini and Merlini, 1986; Cello and Mazzoli, 1998) was
79 affected by thick-skinned tectonics (Butler et al., 2004; Shiner et al., 2004). Differently, its outer
80 portion was affected by a significant bulging and development of a Plio-Pleistocene foreland basin
81 system (Pieri et al., 1997; Borgomano, 2000; Spalluto, 2012; Petrullo et al., 2017).

82 **2.1 Monte Alpi Unit**

83 The Monte Alpi Unit is made up of ca. 2000 m-thick, Middle Jurassic to Lower Cretaceous shallow-
84 water carbonates and of 100's of m-thick Messinian carbonate and terrigenous rocks (Fig. 2; De

85 Lorenzo, 1895; Selli, 1957; Sartoni and Crescenti, 1962; Grandjacquet, 1963; Roda, 1965). The
86 Messinian sedimentary succession is stacked into two intervals (Ortolani and Torre, 1971; Sgrosso et
87 al., 1988; Taddei and Siano, 1992; Van Dijk et al., 2000). The first one consists of Lower Messinian
88 skeletal carbonates, which stand sub-parallel to the Lower Cretaceous carbonates. The second one is
89 made of Upper Messinian terrigenous deposits, lying with a sharp angular unconformity on both
90 Lower Messinian and Lower Cretaceous carbonates. Although debated in the past, the most recent
91 studies attributed the Mesozoic Monte Alpi carbonates to the Inner Apulian Platform (Sgrosso, 1988;
92 Van Dijk et al., 2000; Alberti et al., 2001; Mazzoli et al., 2006; La Bruna et al., 2017, 2018). The whole
93 Monte Alpi Unit was interpreted as a push-up structure associated to Quaternary strike-slip tectonics
94 (Van Dijk et al., 2000), or as a more complex structure due to combined thin- and thick-skinned Plio-
95 Quaternary compressional tectonics and trans-tensional faulting (Shiner et al., 2004; Mazzoli et al.,
96 2006, 2014). Recently, La Bruna et al. (2017) showed that the Monte Alpi structure formed during five
97 deformation stages: 1) foreland bulging and along-foredeep basin stretching, which produced a pre-
98 compressional, high-angle fault system (pre-Pliocene); 2) emplacement of the allochthon by mean of
99 low-angle thrust faults inducing small-scale strike-slip faults in the Apulian carbonates (Early
100 Pliocene); 3) tectonic inversion of the thrust faults in different levels of the allochthon and onset of
101 low-angle faults (Upper Pliocene); 4) left-lateral, strike-slip motion along NW-SE striking faults and
102 extensional reactivation of pre-existing E-W faults (Lower Pleistocene) followed by left-lateral strike-
103 slip motion of N-S striking faults, and coeval formation of NW-SE striking normal faults (Middle
104 Pleistocene); 5) extension and normal slip on most pre-existing faults which significantly raised and
105 exhumed the Monte Alpi Unit (Middle Pleistocene-Holocene).

106

107 **3. Methods**

108 **3.1 Field analysis**

109 We study two sub-vertical outcrops exposing the Lower Cretaceous limestones. The Solarino and
110 Monte Teduro sites are respectively oriented ca. N-S- and NW-SE, and about 2m² in size (Figs. 3a and
111 4a). At each outcrop, detailed stratigraphic logging and qualitative structural analyses aimed at

112 deciphering the nature, attitude, geometry, infill, and abutting/crosscutting relationships of individual
113 fractures are carried out.

114 **3.2 Petrographic and mineralogical analyses**

115 The laboratory work includes the petrographic analysis of 60 thin-sections obtained from hand
116 samples collected in the field (29 from the Solarino site, 31 from the Monte Teduro site). The
117 petrographic analysis was carried out using a polarized light Olympus™ microscope BH2, which is
118 equipped with a digital camera Zeiss™ MRc5. Based on their texture the study rocks were sorted
119 according to Dunham (1962) and Embry and Klovan (1971) classifications. For mineralogical and
120 cement analysis the thin-sections were examined with the cathodoluminescence technique
121 (Technosyn Cold Cathode Luminescence Model 8200Mk II). We assessed the relative timing of
122 individual diagenetic elements according to superposition and overlap principles (Meyers, 1974;
123 Goldstein, 1991; Meyers, 1991; Durllet and Loreau, 1996; Boggs, 2009). Furthermore, sawing of
124 samples reveals further structural elements invisible at outcrop. Accordingly, the slivers of rock
125 samples obtained during thin section preparation were re-oriented in order to measure the main
126 attitude of the small structural elements visible under the optical microscope.

127

128 **4. Results**

129 The Lower Cretaceous carbonates consist of whitish to dark grey limestones arranged in 10's of cm to
130 a few m-thick tabular beds, forming transgressive-regressive depositional depositional sequences
131 dominated by peritidal carbonate facies (Tables 1 and 2) and bounded by bedding-parallel surfaces.
132 The latter appear more prominent than bedding surfaces. Some of them bound a few m-thick bed
133 packages, other bound a few 10's of m-thick beds as documented by Giuffrida et al. (2019b).
134 Accordingly, these surfaces are named Transgressive Surfaces (TSs) and Prominent Transgressive
135 Surfaces (PTSs), (Figs. 3b, 4b, 4c, 4d, 4e). TSs bound a few m-thick depositional sequences and are
136 interpreted as 3rd order sequence boundaries (Spalluto, 2012; Rustichelli et al., 2016; Panza et al.,
137 2016; Giuffrida et al., 2019b). PTSs bound 10's of meters thick depositional sequences and are
138 interpreted as 2nd order sequence boundaries (Spalluto, 2012; Giuffrida et al., 2019b) associated to
139 tectonics and/or global sea level changes (Strasser et al., 1999).

140 **4.1 Mesoscale analysis**

141 The two study sites of Solarino and Monte Teduro expose 4 to 60 cm-thick, greyish limestone beds
142 dipping 15° SSE and 30° SE, respectively (Figs. 3c, 3d, 4c, 4d, 4e). The high-resolution mapping shows
143 the following fracture sets:

- 144 • bed-perpendicular, strata bound joints and sheared joints striking N-S and E-W, and
145 dipping > 70°E and N, respectively (Figs. 3e, 3f, 3g, 4f, 4g, 4h);
- 146 • bed-parallel stylolites (Figs. 3e, 3f, 3g, 4f, 4g, 4h);
- 147 • oblique-to-bedding joints and sheared joints ENE-WSW-striking and ~50° SSE-dipping,
148 (Figs. 3e, 3f, 3g, 4f, 4g, 4h). In some cases, these oblique-to-bedding structural elements
149 linked bed-perpendicular joints, forming non-strata bound incipient slip surfaces
150 which offset bed interfaces up to a few centimetres ;
- 151 • sub-vertical joints and sheared joints striking NNW-SSE, which either crosscut or abut
152 against the sub-horizontal stylolites (Figs. 3e, 3f, 3g, 4f, 4g, 4h);
- 153 • sub-horizontal stylolites, which always abut against the bed-parallel stylolites (Figs. 3e,
154 3f, 3g, 4f, 4g, 4h).

155 **4.2 Petrographic analysis**

156 Thin-section analysis was key to decipher the carbonate texture originally formed on a flat-topped
157 carbonate platform (Fig. 5, Tables 1 and 2). According to their texture, we document a variety of
158 microfacies from wackestones to floatstones and bindstones (Dunham, 1962). Dominant biota and
159 allochems are benthic foraminifera, bivalve bioclasts, ostracods and oncoids. Dasycladacean green
160 algae, gastropods and peloids are less common. Intraformational, oncoïd-bearing, angular lithoclasts
161 exclusively occur in Bed 0 (Monte Teduro site), which is bounded by a PTS. Sedimentary and biogenic
162 structures include bed-parallel stromatolitic lamination in microbial bindstones, and fenestral features
163 (original fenestrae-type pores now are filled with blocky calcite). Bioturbations such as burrows and
164 borings occur in Monte Teduro site.

165 Among the diagenetic products, the microsparry-to-sparry calcite cement is ubiquitous in all
166 microfacies. It is characterized by a dominant blocky texture that destroyed the primary host rock
167 porosity. This frequently patchily distributed cement fills fenestral and bioturbation features, as well

168 as the topmost part of geopetal features. Their basal part is filled by a vadose silt. Isopachous calcite
169 cements around grains also occur. Sparse dolomite crystals and recent vuggy pores are rare.

170 **4.3 Microstructural analysis**

171 Microstructural analysis revealed the following assemblages:

- 172 • Calcite micro-veins ~E-W-striking and ~70°N-dipping, often compartmentalized by
173 fenestral features and/or bioturbation-related bores (Figs. 6a, 6b, 6c, 7a and 7b);
- 174 • cross-orthogonal, bed-perpendicular calcite veins N-S- and E-W- striking, respectively
175 70°N- and S- dipping (Figs. 8a, 8b, 8c, 8d and 9a), cutting across bioturbation-related bores,
176 and abutting against bed-parallel stylolites (Figs. 6a, 6b, 6c, 6d, 8a, 8b, 8c and 8d).
- 177 • bed-parallel calcite veins that crosscut bed-perpendicular veins (Figs. 6a, 6b, 6c, 6d, 7a, 7b,
178 7d, 8a, 8b, 8c, 8d, 9a, 9b and 9d);
- 179 • bed-perpendicular stylolites, which show mutual abutting relationships with the bed-
180 parallel veins (Figs. 6a, 6b, 6c, 6d, 8a, 8b, 8c and 8d);
- 181 • oblique-to-bedding calcite veins striking ENE-WSW, dipping > 60° SSE, abutting against the
182 bed-perpendicular veins and either crosscutting or terminating against the bed-parallel
183 veins (Figs. 6a, 6b, 6c, 6d, 7c, 8a, 8b, 8c, 8d, 9c and 9d);
- 184 • sub-vertical calcite veins striking NNW-SSE, dipping > 80° WSW, crosscutting all
185 aforementioned structures (Figs. 6a, 6b, 6c, 6d, 7d, 8a, 8b, 8c, 8d and 9b), and in some cases
186 abutting against the sub-horizontal stylolites (Figs. 6a, 6b, 6c and 6d);
- 187 • sub-horizontal calcite veins, which either crosscut or abut against all previous structures
188 (Figs. 6a, 6b, 6c, 6d, 7d, 7e, 8a, 8b, 8c, 8d, 9b, 9c and 9d), and compartmentalized by high
189 angle-to-bedding stylolites (Figs. 6a, 6b, 6c and 6d);
- 190 • sub-vertical calcite veins striking NW-SE, dipping > 85° SW, crosscutting all previous
191 structures (Figs. 8a, 8b, 8c, 8d and 9d).

192

193 **5. Data Interpretation**

194 The diagenetic evolution of the Monte Alpi limestones is assessed on petrographic observations under
195 both planar- and cross-polarized lights, coupled with cathodoluminescence analysis of thin sections.
196 According to the principles of Meyers (1974; 1991) our interpretation is proposed as follows.

197 **5.1 Diagenetic evolution**

198 Seven diagenetic stages are assessed:

- 199 • The Early Calcite Cementation event (EC) is marked by isopachous, non-ferroan, euhedral,
200 limpid calcite cement with crystal sizes between 50 and 400 μm . This cement is
201 characterized by poor luminescence, from black to brown dull. It coats the grains and
202 localizes inside bioturbation bores and on top of the geopets (Figs. 10 and 11). This
203 cement is typical of an early diagenetic fabric (Choquette and Pray, 1970). Other evidence
204 for EC occurs in the mud-supported samples where fenestrae and microveins are filled
205 with blocky calcite (Figs. 7a, 7b, 9a and 9b).
- 206 • The second stage is marked by the Calcite cement 1 (Cal1). It is a non-ferroan cement made
207 of limpid crystals (Figs. 9a and 9b). Under cathodoluminescence, Cal1 cements have a non-
208 luminescent core of 50-200 μm and a light bright-to-orange, luminescent, fringe 5-to-10
209 μm in size. Cal1 fills the cross-orthogonal, bed-perpendicular veins (Figs. 9a and 9b).
- 210 • The third stage is characterized by a Calcite cement 2 (Cal2) which consists of a drusy-to-
211 mosaic spar that fills bed-parallel veins and some intragranular pores. In planar polarized
212 light, the calcite crystals are subhedral to euhedral, limpid, and 10-to-50 μm in size. In CL,
213 Cal2 comprises two phases Cal2a and Cal2b. Cal2a is non-ferroan, non-luminescent, from
214 black to dull brown calcite (Figs. 7c, 7c1 and 7d). Cal2b is made of dull brown ferroan
215 luminescent crystals, bordered by orange-to-bright yellow luminescent fringes (Figs. 7a,
216 7b, 7c, 7c1, 7d, 9a, 9b, and 9d).
- 217 • The fourth stage is associated to the calcite cement 3 (Cal3), which fills the oblique-to-
218 bedding veins striking ENE-WSW. It is a limpid, subhedral-to-euhedral, 10-to-200 μm in
219 size calcite (Figs. 7c, 9a and 9d). Crystal cores are mostly ferroan and show a bright orange
220 luminescence under CL (Figs. 7c, 9c and 9d);

- 221 • Stage five is marked by the calcite cement 4 (Cal4) which fills the oblique-to-bedding veins
 222 striking NNW-SSE (Figs. 7d and 9b). Cal4 is limpid, subhedral and euhedral with sizes
 223 ranging between 10 and 50 μm . Under CL, Cal4 is bright brown to bright luminescent (Figs.
 224 7d and 9b).
- 225 • The sixth stage is associated to the calcite cement 5 (Cal5) which occurs in sub-horizontal
 226 veins (Figs. 7d, 9c and 9d). Cal5 is subhedral and euhedral, limpid, ranging from 10 to 50
 227 μm in size. In CL, it is orange-to-yellow bright (Figs 7d, 7e, 9b, 9c and 9d).
- 228 • The seventh stage is marked by the calcite cement 6 (Cal6) which occurs in sub-vertical
 229 veins striking NW-SE. The ferroan calcite is made of 10-to-100 μm in size, turbid brown
 230 and limpid crystals (Figs. 9d). These crystals are dark red-to-orange luminescent under CL,
 231 (Figs. 9c and 9d).

232 5.2 Structural evolution

233 In this section, on the basis of the aforementioned diagenetic history, we assessed the time-dependant
 234 structural evolution of the study studied limestones by considering both field and laboratory data (Fig.
 235 12):

- 236 • The oldest structures are the very tiny E-W veins filled with EC blocky calcite which also
 237 filled intragranular pores (J0, Figs. 12a and 12b). Some samples bear micro-veins that abut
 238 against early fenestral features which were also cemented by EC (Figs. 7a and 7b).
- 239 • The bed-perpendicular, cross-orthogonal joints and veins (J1) and the bed-parallel
 240 stylolites (S1) show mutual abutting relationships (Figs. 12a and 12c) are interpreted as
 241 coeval (Bai et al., 2002.). Bed-perpendicular veins crosscut early diagenetic features such
 242 as bioturbation and J0 microveins filled with EC blocky calcite. Hence, they J1 postdate J0.
 243 J1 veins are filled with Cal1 characterized by non-luminescent cores, and by bright orange
 244 luminescent fringes (Figs. 9a and 9b). This evidence denotes a progressive chemical change
 245 compared to earliest stage.
- 246 • The bed-parallel veins (J2) and bed-perpendicular stylolites (S2) exhibit mutual abutting
 247 relationships (Figs. 12a and 12d), crosscut both J0 and J1 and are filled with Cal2 cements
 248 (Figs. 6b, 6c, 7a, 7b, 7c, 8b, 8c, 9a and 9b). Since Cal2 displays an alternation of dull brown

249 non-luminescent cores (Cal2a, Figs. 7c, 7c1 and 7d) and bright luminescent fringes (Cal2b,
250 Figs. 7a, 7b, 7c, 7c1, 7d, 9a, 9b and 9d), the formation of J2 and S2 is ascribed to telogenesis.
251 There, oxidizing and reducing conditions likely alternated (Richter et al., 2003; Boggs and
252 Krinsley, 2006; Hiatt and Pufahl, 2014).

- 253 • The oblique-to-bedding veins (J3) abut against J1 (Figs. 3f, 4g, 12a and 12e) and J2 (Figs.
254 6b, 6c, 7c, 8b, 8c, 9c and 9d) at both meso- and micro-scales. J3 are filled with Cal3 cements
255 which display orange, bright luminescence consistent with reducing conditions (Richter et
256 al., 2003). Accordingly, J3 likely formed during gently increased burial depth with respect
257 to the previous stage.
- 258 • Both NNW-SSE-striking oblique-to-bedding joints/veins (J4) and sub-horizontal stylolites
259 (S4) show mutual abutting relationship at the outcrop scale (Figs. 3e, 3f, 4f, 4g, 12a and
260 12f) and crosscut all aforementioned structures at microscale (Figs. 6b, 6c, 7d, 8b, 8c and
261 9c). Since they are filled with Cal5 cements, which are characterized by yellow bright
262 luminescence (Fig. 12), we interpret that J4 formed under reducing conditions (Boggs and
263 Krinsley, 2006) in deep burial diagenetic environments (Hiatt and Pufahl, 2014).
- 264 • At microscale, sub-horizontal veins (J5) and high-angle to bedding stylolites (S5) show
265 mutual abutting relationships and crosscut all aforementioned structures (Figs. 6b, 6c, 7d,
266 8b, 8c, 9c, 9d, 12a and 12g). J5 is filled with Cal5 cements displaying bright orange/yellow
267 luminescence. Therefore, it likely formed under reducing conditions (Boggs and Krinsley,
268 2006) in burial diagenetic environments (Hiatt and Pufahl, 2014).
- 269 • The most recent structures are sub-vertical joints and veins (J6). At micro-scale they
270 crosscut all previous structures (Figs. 8b, 8c, 9d, 12a and 12h). They are cemented by Cal6
271 having bright orange luminescence and, hence, formed under reducing conditions (Boggs
272 and Krinsley, 2006).

273

274 **6. Discussion**

275 **6.1 Micro-to-meso scale structural assemblages**

276 Both field and laboratory data obtained for the limestones cropping out at the Solarino and Monte
277 Teduro sites are hereafter considered in light of the existing bibliography in order to discuss the
278 deformation mechanisms, geometry and fracture network according to the polyphase tectonic
279 evolution of the Monte Alpi Unit, with a special focus on the modalities of carbonates early
280 embrittlement.

281 The main structural assemblages deciphered for the study are the following:

282 (0) *Early embrittlement assemblage*. The first assemblage is made up by the J0 structural elements,
283 which were strictly related to the EC processes that caused the blocky calcite precipitation in
284 the most fine-grained portions of the sedimentary pile (Fig. 12b). EC occurred during Lower
285 Cretaceous times, when the carbonate sediments experienced shallow marine to meteoric
286 diagenesis (Figs. 13b and 13c).

287 (1) *First burial assemblage*. It includes both J1 and S1 which formed during Cretaceous times when
288 the burial progressively increased (Corrado et al., 2002). Both sets of cross-orthogonal bed-
289 perpendicular joint and veins (J1a and J1b) strike E-W and N-S (Figs. 4, 6, 8 and 13c). They
290 show mutual abutting relationships with respect to the bed-parallel stylolites (La Bruna et al.
291 2017-2018; Giuffrida et al., 2019a). By considering that, J1 sets are filled with Cal1 cements,
292 their sealing occurred under phreatic conditions, when cements contained higher divalent Mn,
293 and low Fe concentrations (Boggs and Krinsley, 2006). Therefore, we ascribe a burial-related
294 origin for the Cal1 cement (Bathurst, 1975; Tucker et al., 1990; Lavenu and Lamarche 2018)
295 occurred during mesogenesis (Figs. 12a and 13b) in the sense of Choquette and Pray (1970).
296 The coeval formation of cross-orthogonal bed-perpendicular joints induces an asset up under
297 vertical σ_1 and horizontal $\sigma_2 \approx \sigma_3$ principal stress axes (Bai and Pollard, 2000; Bai et al., 2002)
298 during mesogenesis (Figs. 12a, 13b and 13c). This brittle mechanism was already documented
299 by Agosta and Aydin (2006), Agosta et al., (2010, 2012), Rustichelli et al., (2013, 2016), Lavenu
300 et al., (2014, 2015), and Korneva et al. (2014) and Panza et al. (2015, 2016) for tight
301 carbonates cropping out in central and southern Italy, and in south-eastern Spain.

302 (2) *Layer Parallel Shortening Assemblage*. This assemblage includes bed-parallel veins (J2) and
303 bed-perpendicular stylolites (S2), which formed during Miocene times (Figs. 13b and 13c) in

304 sub-horizontal limestone beds. Bed-parallel joints were filled with non-ferroan and non-
305 luminescent calcite whose precipitation could be ascribed to the pre-Messinian times during
306 the first telogenesis culmination (Cal2a; figs. 7c, 7c1 and 7d). This structural assemblage was
307 likely associated to the far field propagation of horizontal compressive stresses related to the
308 migrating Southern Apennines FTB thrust front (sensu Geiser and Engelder, 1983). Differently,
309 bed-parallel joints filled with Cal2b calcite, which displays a bright luminescence in CL (Figs.
310 7a, 7b, 7c, 7c1, 7d, 9a, 9b and 9d), likely formed during Early Messinian in the back-bulge
311 marine deposition zone of the foreland basin system (La Bruna et al., 2018). Quite similar
312 structural assemblage was documented in the Outer Apulian Platform of Italy, both in
313 carbonates platform (Graham et al., 2003; Aydin et al., 2010; Rustichelli et al., 2016), and ramp
314 (Antonellini et al., 2008; Agosta et al., 2009, 2010; Rustichelli et al., 2012). However, the
315 present study document for the first time the occurrence of bed-parallel veins in the Apulian
316 carbonates. These structures were described in Jurassic tight limestones of the Lazio-Abruzzi
317 Platform of central Italy by Agosta and Aydin (2006) and Agosta et al. (2008), who interpreted
318 them as part of the thrust-assemblage due to transients of high fluid pressure conditions that
319 exceeded the vertical loading (sensu Hubbert and Rubey, 1959).

320 (3) *Foredeep Basin System Assemblage*. This assemblage includes J3 structural elements (Fig. 13c)
321 related to the Late Messinian tectonic evolution of the Monte Alpi foredeep basin, which took
322 place during Late Messinian times synchronous with the deposition of an up to 300 m-thick
323 sedimentary succession (Patacca et al., 1992; La Bruna et al., 2018; Figs. 13a and 13b). We
324 attribute the J3 formation to localized stress fields due to the shearing of pre-existing
325 structural heterogeneities. Indeed, J3 are envisioned as fault-related structural elements,
326 which cluster at the mode II termination of sheared fracture tip zones, forming splay
327 joints/veins, or at their mode III terminations, forming en-echelon arrays (Figs. 4f and 4g). At a
328 larger scale, this structural configuration was documented by Giuffrida et al. (2019b) in nearby
329 outcrops of the Monte Alpi, and by many other authors in the Outer Apulian Platform
330 carbonates of central and southern Italy (ie., Korneva et al., 2015; Panza et al., 2018, and
331 references therein).

332 (4) *Tectonic burial assemblage*. During Early Pliocene, the tectonic load related to the juxtaposition
333 of the Southern Apennines FTB onto the Apulian carbonates (Cello and Mazzoli 1998; Patacca
334 and Scandone 2007; Tavani et al., 2015) led to the formation of J4 and S4 structures. Hence,
335 they are interpreted as due to a second burial event of the Monte Alpi carbonates (Figs. 13a to
336 13c). Since coeval Cal4 cements display bright brown to bright yellow luminescent colours
337 (Figs. 7d and 9b), we assess that the precipitation took place under reducing conditions at
338 depths of 5-6 km (Corrado et al., 2002; Mazzoli et al., 2006).

339 (5) *Deep-seated thrusting assemblage*. During Late Pliocene times, S5 and J5 structures formed
340 when deep-seated reverse faulting affected the Monte Alpi Unit (Shiner et al., 2004; Mazzoli et
341 al., 2006; Mazzoli et al., 2008) (Figs. 13a to 13c). Deep burial conditions are inferred and
342 supported by the bright orange luminescence of J5 micro-veins (Figs. 7e, 9b, 9c and 9d). We
343 therefore document the aforementioned structural elements in the Apulian carbonates,
344 whereas their occurrence was previously assessed by Agosta and Aydin (2006) for the Jurassic
345 limestones of Lazio-Abruzzi carbonate Platform exposed in central Italy.

346 (6) *Polyphase transpressional/extensional exhumation assemblage*. The last assemblage includes J6
347 that formed during the latest tectonic stages (Mazzoli et al., 2014; La Bruna et al., 2017, 2018);
348 which crosscut all previous assemblages (Figs. 9c and 9d) and were dilated during exhumation
349 from depth (Figs. 13a to 13c). Similar structures were documented throughout the whole
350 Outer Apulian Platform exposed in central and southern Italy (Korneva et al., 2014; Panza et
351 al., 2016).

352 **6.2 Early structural diagenesis**

353 We know that platform carbonates are commonly affected by early diagenetic modifications
354 (Anselmetti and Eberli, 1993) which may increase their stiffness in case of Early Cementation, EC
355 (Eberli et al., 2003). In the Monte Alpi Unit, we documented that in carbonate mudstones early
356 cements filled pores associated to either bioturbation or to fenestral porosity (Figs. 10 and 11). The
357 carbonate mud intervals were originally deposited in a back-reef inner platform/platform margin
358 setting (cf. Figs. 9a and 9b), and were affected by a EC processes that took place at the water-sediment
359 interface or at very shallow depth enhanced by micro-organisms on living organisms and calcite grains

360 (Bathurst 1975). These micro-organisms perforated the calcitic envelope of the original grains, and
361 triggered micritization at the onset of eogenesis (Tucker et al., 1990).

362 In the mud-supported lithified sediments, early embrittlement took place prior to bioturbation
363 (boring) of hard substrates (cf. thin sections T0Bb, T6a, T7b, and T8d, Table 2, and Fig. 5d).
364 Accordingly, we envision that both dissolution cavities (vuggy porosity *sensu* Choquette and Pray,
365 1970) and blocky cements formed during transients of platform emersions. They were therefore,
366 subjected to meteoric diagenesis, then partially obliterated by the bores during the subsequent marine
367 transgressions. Hence, EC processes led to rapid lithification and embrittlement of selective portions
368 of the carbonate pile, which was affected by localized brittle failure and pressure solution (Nelson,
369 1981, 2001; Wennberg et al., 2006; Rustichelli et al., 2012, 2013, 2015; Lavenu et al., 2015, 2018).
370 These results show that the subsequent mechanical behaviour of the studied limestones is also related
371 to their very early diagenetic evolution, which controlled the initial lithification of the carbonate muds.

372 **7. Conclusions**

373 The present study combined field and laboratory analyses to reconstruct the nature and timing of
374 fracture networks in Lower Cretaceous limestones exposed at the Monte Alpi, southern Italy. We first
375 deciphered both diagenetic and structural evolution of the limestones, and then proposed a conceptual
376 model related to the time-dependant evolution of the structural assemblages in light of the complex
377 tectonic history of the southern Apennines. We focussed on the early cementation processes
378 responsible for the onset of joints and veins at very shallow burial conditions. These processes played
379 a fundamental role on subsequent development of the present-day mechanical and fracture
380 stratigraphy. Specifically, we assessed the following assemblages:

- 381 (0) early embrittlement assemblage (Lower Cretaceous) ascribed to a first stage of eogenesis
382 characterized by early calcite cementation processes and fracture development in the mud-
383 rich portions of the carbonate pile;
- 384 (1) first burial assemblage (Cretaceous) related to the growth of the Inner Apulian Platform and
385 the progressive burial which caused the formation of bed-parallel stylolites and two sets of
386 cross-orthogonal bed-perpendicular joints and veins;

- 387 (2) layer parallel shortening assemblage (pre-Messinian) due to the FTB far field stress
388 propagation within the Inner Apulian Platform, and characterised by one set of bed-
389 perpendicular stylolites and bed-parallel veins;
- 390 (3) foredeep basin system assemblage (Late Messinian) related to fault activity during the
391 structural evolution of the Monte Alpi foreland basin system, and composed of NW-SE striking
392 joints and veins;
- 393 (4) tectonic burial assemblage (Early Pliocene) due to the tectonic loading of the southern
394 Apennines allochthon and made up of oblique-to-bedding joint, veins and stylolites.
- 395 (5) deep-seated thrusting assemblage (Late Pliocene) due to steep reverse faults, and made up of
396 sub-vertical stylolites and low-angle joints and veins;
- 397 (6) polyphase transpressional/extensional exhumation assemblage (Early Pleistocene to
398 Holocene) related to strike-slip faulting and the latest rock exhumation. It comprises sub-
399 vertical joints and veins that crosscut all previous structural assemblages.

400 We assessed that early calcite (EC) precipitation mainly occurred within mud-rich carbonate
401 sediments. Both pore dimensions and texture variations were factors driving EC processes in
402 carbonates. We concluded that localized early embrittlement of carbonates determined the
403 subsequent early fractures nucleation in mudstones beds and provided new insights into the
404 mechanical control and nucleation of diffuse fractures. Therefore, these diffuse fractures providing the
405 background permeability in naturally fractured carbonate reservoirs are due to early burial diagenesis
406 that cause the stiffening of the finer grained portions of the carbonate pile.

407

408 **Acknowledgments**

409 VLB acknowledges Giacomo Prosser, Anthony Tendil, and Paola Castelluccio for the support provided
410 during field and laboratory analyses, and Christophe Matonti for the interesting and useful discussion
411 on timing of structural diagenesis. The detailed revision provided by Dr. Arthur Lavenu and by an
412 anonymous reviewer sensitively improved the quality of the manuscript. This work was co-financed
413 by the Vinci Program (Université Franco-Italienne), and by the Reservoir Characterization Project
414 (www.rechproject.com).

415

416 **Bibliography**

- 417 Agosta, F., Aydin, A., 2006. Architecture and deformation mechanism of a basin bounding normal fault
418 in Mesozoic platform carbonates, central Italy. *Journal of Structural Geology*, 28, 1445-1467.
- 419 Agosta, F., Mulch, A., Chamberlain, P., Aydin, A., 2008. Geochemical traces of CO₂-rich fluid flow along
420 normal faults in central Italy. *Geophysical Journal International*, 174, 758-770.
- 421 Agosta, F., Alessandrini, M., Tondi, E., Aydin, A., 2009. Oblique normal faulting along the northern edge of
422 the Majella anticline, central Italy: Inferences on hydrocarbon migration and accumulation. *Journal of*
423 *Structural Geology*, 31, 674-690.
- 424 Agosta, F., Alessandrini, M., Antonellini, M., Tondi, E., Giorgioni, M., 2010. From fractures to flow: a
425 field-based quantitative analysis of an outcropping carbonate reservoir. *Tectonophysics*, 490, 197-
426 213.
- 427 Agosta, F., Ruano, P., Rustichelli, A., Tondi, E., Galindo-Zaldívar, J., De Galdeano, C. S., 2012. Inner
428 structure and deformation mechanisms of normal faults in conglomerates and carbonate
429 grainstones (Granada Basin, Betic Cordillera, Spain): inferences on fault permeability. *Journal of*
430 *Structural Geology* 45, 4-20.
- 431 Agosta, F., Wilson, C., Aydin, A., 2015. The role of mechanical stratigraphy on normal fault growth
432 across a Cretaceous carbonate multi-layer, central Texas (USA). *Italian Journal of Geosciences*, 134,
433 423-441.
- 434 Alberti, M., Lapenta, M.C., Maurella, A., 2001. New geological data on the basin units surrounding the
435 Monte Alpi unit (southern Italy). *Bollettino della Società dei Naturalisti in Napoli - Nuova Serie*, 1,
436 85-96.
- 437 Anders, M. H., Laubach, S. E., Scholz, C. H., 2014. Microfractures: A review. *Journal of Structural*
438 *Geology*, 69, 377-394.
- 439 Anselmetti, F. S., Eberli, G. P., 1993. Controls on sonic velocity in carbonates. *Pure and Applied*
440 *geophysics*, 141, 287-323.

- 441 Antonellini, M., Tondi, E., Agosta, F., Aydin, A., Cello, G., 2008. Failure modes in deep-water carbonates and
442 their impact for fault development: Majella Mountain, Central Apennines, Italy. *Marine and Petroleum*
443 *Geology*, 25, 1074-1096.
- 444 Aguilera, R., 1998. Geologic aspects of naturally fractured reservoirs. *The Leading Edge*, 17, 1667-
445 1670.
- 446 Ahr, W.M., 2011. *Geology of carbonate reservoirs: the identification, description and characterization of*
447 *hydrocarbon reservoirs in carbonate rocks*. John Wiley & Sons.
- 448 Aydin, A., Antonellini, M., Tondi, E., Agosta, F., 2010. Deformation along the leading edge of the Maiella
449 thrust sheet in central Italy. *Journal of Structural Geology*, 32, 1291-1304.
- 450 Bai, T., Pollard, D. D., 2000. Fracture spacing in layered rocks: a new explanation based on the stress
451 transition. *Journal of Structural Geology* 22, 43-57.
- 452 Bai, T., Maerten, L., Gross, M. R., Aydin, A., 2002. Orthogonal cross joints: do they imply a regional
453 stress rotation? *Journal of Structural Geology* 24, 77-88.
- 454 Barbier, M., Hamon, Y., Callot, J.P., Floquet, M., Daniel, J.M., 2012. Sedimentary and diagenetic controls
455 on the multiscale fracturing pattern of a carbonate reservoir. The Madison formation (Sheep
456 Mountain, Wyoming, USA): *Marine and Petroleum Geology* 29, 50-67.
- 457 Barlet-Gouedard, V., Rimmelé, G., Goffe, B., Porcherie, O., 2006. Mitigation strategies for the risk of CO₂
458 migration through wellbores. In IADC/SPE drilling conference. Society of Petroleum Engineers.
- 459 Bathurst, R.G., 1972. *Carbonate sediments and their diagenesis*. Vol. 12. Elsevier.
- 460 Boggs, S., Krinsley, D., 2006. *Application of cathodoluminescence imaging to the study of sedimentary*
461 *rocks*. New York, NY, Cambridge University Press, 176p
- 462 Boggs, S., 2009. *Petrology of sedimentary rocks*. New York, NY, Cambridge University Press, 600p.
- 463 Bonardi, G., D'argenio, B., Perrone, V., 1988. *Carta Geologica dell'Appennino Meridionale in scala 1:*
464 *250.000*.
- 465 Borgomano, J. R. F., 2000. The Upper Cretaceous carbonates of the Gargano-Murge region, southern
466 Italy: a model of platform-to-basin transition. *AAPG Bulletin* 84, 1561-1588.
- 467 Butler, R.W.H., Mazzoli, S., Corrado, S., De Donatis, M., Scrocca, D., Di Bucci, D., Gambini, R., Naso, G.,
468 Nicolai, C., Shiner, P., Zucconi, V., 2004. Applying thick-skinned tectonic models to the Apennine

- 469 thrust belt of Italy – Limitations and implications. In: Thrust tectonics and hydrocarbon systems
470 (K.R. McClay, ed.). American Association of Petroleum Geologists 82, 647-667.
- 471 Carbone, S., Catalano, S., Lentini, F., Monaco, C., 1988. Le unità stratigrafico-strutturali dell'Alta Val
472 d'Agri (Appennino lucano) nel quadro dell'evoluzione del sistema catena-avanfossa. Memorie
473 Società Geologica Italiana 41, 331-341.
- 474 Cavazza, W., Roure, F., Ziegler, P., 2004. The Mediterranean Area and the Surrounding Regions: Active
475 Processes, Remnants of Former Tethyan Oceans and Related Thrust Belts. In: W. Cavazza, F. Roure,
476 W. Spakman, G.M. Stampfli and P. Ziegler (Eds). The TRANSMED Atlas, 1-29.
- 477 Cello, G., Mazzoli, S. 1998. Apennine tectonics in southern Italy: a review. Journal of Geodynamics, 27,
478 191-211.
- 479 Choquette, P.W., Pray, L.C., 1970. Geologic nomenclature and classification of porosity in sedimentary
480 carbonates. AAPG bulletin, 54, 207-250.
- 481 Corradetti, A., Tavani, S., Parente, M., Iannace, A., Vinci, F., Pirmez, C., Torrieri, S., Giorgioni M.,
482 Pignalosa A., Mazzoli, S., 2018. Distribution and arrest of vertical through-going joints in a seismic-
483 scale carbonate platform exposure (Sorrento peninsula, Italy): insights from integrating field
484 survey and digital outcrop model. Journal of Structural Geology, 108, 121-136.
- 485 Corrado, S., Invernizzi, C., Mazzoli, S., 2002. Tectonic burial and exhumation in a foreland fold and
486 thrust belt: The Alpi Mt. case history (Southern Apennines, Italy). Geodinamica Acta 15, 159-177.
- 487 De Lorenzo, G., 1895. Osservazioni geologiche nell'Appennino della Basilicata meridionale. Atti
488 Accademia di Scienza Fisica. Materiali 27, 31.
- 489 Cosentino, D., Cipollari, P., & Pipponzi, G. (2003). Il sistema orogenico dell'Appennino centrale: vincoli
490 stratigrafici e cronologia della migrazione. In: Cipollari, P., Cosentino, D. (Eds.), Evoluzione
491 cinematica del sistema orogenico dell'Appennino centro-meridionale: caratterizzazione
492 stratigrafico-strutturale dei bacini sintettonici. Studi Camerti, Numero Speciale 2003, 85-99.
- 493 Doglioni, C., 1991. A proposal for kinematic modeling of W-dipping subductions - Possible applications
494 to the Tyrrhenian-Appennines system. Terra Nova 3, 423-434.
- 495 Dunham, R., 1962. Classification of Carbonate Rocks According to Depositional Textures. In W.E. Ham,
496 Classification of carbonate rocks. AAPG Memoir 1, 108-121.

- 497 Durllet, C., Loreau, J. P., 1996. Séquence diagénétique intrinsèque des surfaces durcies: mise en
498 évidence de surface d'émersion et de leur ablation marine. Exemple de la plate-forme
499 bourguignonne, Bajocien (France). Comptes rendus de l'Académie des sciences. Série 2. Sciences de
500 la terre et des planètes, 323, 389-396.
- 501 Eberli, G.P., Baechle, G.T., Anselmetti, F.S., Incze, M.L., 2003. Factors controlling elastic properties in
502 carbonate sediments and rocks. *The Leading Edge*, 22, 654-660.
- 503 Embry, A. F., Klovan, J. E., 1971. A late Devonian reef tract on northeastern Banks Island, NWT. *Bulletin*
504 *of Canadian Petroleum Geology*, 19, 730-781.
- 505 Ford, D.C., Williams, P.W., 2007. *Karst hydrogeology and geomorphology*. Chichester: John Wiley & Sons,
506 Vol. 576.
- 507 Frost, E.L., Kerans, C., 2010. Controls on syndepositional fracture patterns, Devonian reef complexes,
508 Canning Basin, Western Australia. *Journal of Structural Geology*, 32, 1231-1249.
- 509 Geiser, P., Engelder, J. T., 1983. The distribution of layer parallel shortening fabrics in the Appalachian
510 foreland of New York and Pennsylvania: Evidence for two non-coaxial phases of the Alleghanian
511 orogeny. *Memoir of the Geological Society of America*, 158, 161-175.
- 512 Giorgioni, M., Iannace, A., D'Amore, M., Dati, F., Galluccio, L., Guerriero, V., Mazzoli S., Parente M.,
513 Strauss, C., Vitale, S., 2016. Impact of early dolomitization on multi-scale petrophysical
514 heterogeneities and fracture intensity of low-porosity platform carbonates (Albian-Cenomanian,
515 southern Apennines, Italy). *Marine and Petroleum Geology*, 73, 462-478.
- 516 Giuffrida, A., La Bruna, V., Castelluccio, P., Panza, E., Rustichelli, A., Tondi, E., Giorgioni M. Agosta, F.,
517 2019a. Fracture simulation parameters of fractured reservoirs: Analogy with outcropping
518 carbonates of the Inner Apulian Platform, southern Italy. *Journal of Structural Geology*, 123, 18-41.
- 519 Giuffrida, A., Agosta, F., Rustichelli, A., Panza, E., La Bruna, V., Eriksson, M., Torrieri, S., Giorgioni, M.,
520 2019b. Fracture stratigraphy and DFN modelling of tight carbonates, the case study of the Lower
521 Cretaceous carbonates exposed at the Monte Alpi (Basilicata, Italy), *Marine and Petroleum*
522 *Geology*, 104045, ISSN 0264-8172, <https://doi.org/10.1016/j.marpetgeo.2019.104045>
- 523 Ghisetti, F., Vezzani, L., 1997. Interfering paths of deformation and development of arcs in the fold-
524 and-thrust belt of central Apennines (Italy). *Tectonics* 16, 523-536.

- 525 Goldstein, R.H., 1991. Practical aspects of cement stratigraphy with illustrations from Pennsylvanian
526 limestone and sandstone, New Mexico and Kansas. *SEPM Short Course Notes* 25, 123-131, 190-191.
- 527 Grandjacquet, C., 1963. Schéma structural de l'Apennin campano-lucanien (Italie). *Revue de*
528 *Géographie Physique et de Géologie Dynamique* 25, 185-202.
- 529 Graham, B., Antonellini, M., Aydin, A., 2003. Formation and growth of normal faults in carbonates
530 within a compressive environment. *Geology* 31, 11-14.
- 531 Guerriero, V., Mazzoli, S., Iannace, A., Vitale, S., Carravetta, A., Strauss, C., 2013. A permeability model
532 for naturally fractured carbonate reservoirs. *Marine and Petroleum Geology*, 40, 115-134.
- 533 Guerriero, V., Dati, F., Giorgioni, M., Iannace, A., Mazzoli, S., Vitale, S., 2015. The role of stratabound
534 fractures for fluid migration pathways and storage in well-bedded carbonates. *Italian Journal of*
535 *Geosciences*, 134, 383-395.
- 536 Hiatt, E.E., and Pufahl, P.K., 2014. Cathodoluminescence petrography of carbonate rocks: a review of
537 applications for understanding diagenesis, reservoir quality and pore system evolution. *Short*
538 *Course*, 45, 75-96.
- 539 King Hubbert, M., Rubey, W.W., 1959. Role of fluid pressure in mechanics of overthrust faulting: I.
540 Mechanics of fluid-filled porous solids and its application to overthrust faulting. *Geological Society*
541 *of America Bulletin*, 70, 115-166.
- 542 Korneva, I., Tondi, E., Agosta, F., Rustichelli, A., Spina, V., Bitonte, R., Di Cuia, R., 2014. Structural
543 properties of fractured and faulted Cretaceous platform carbonates, Murge Plateau (southern
544 Italy). *Marine and Petroleum Geology*, 57, 312-326.
- 545 Korneva, I., Cilona, A., Tondi, E., Agosta, F., Giorgioni, M., 2015. Characterisation of the permeability
546 anisotropy of Cretaceous platform carbonates by using 3D fracture modeling: the case study of Agri
547 Valley fault zones (southern Italy). *Italian Journal of Geosciences*, 134, 396-408.
- 548 La Bruna, V., Agosta, F., Prosser, G., 2017. New insights on the structural setting of the Monte Alpi area,
549 Basilicata, Italy. *Italian Journal of Geosciences*. 136, 220-237.
- 550 La Bruna, V., Agosta, F., Lamarche, J., Viseur, S., Prosser, G. 2018. Fault growth mechanisms and scaling
551 properties in foreland basin system: The case study of Monte Alpi, Southern Apennines,
552 Italy. *Journal of Structural Geology*, 116, 94-113.

- 553 Lamarche, J., Lavenu, A.P.C., Gauthier, B.D.M., Guglielmi, Y., Jayet, O., 2012. Relationships between
554 fracture patterns, geodynamics and mechanical stratigraphy in Carbonates (South-East Basin,
555 France). *Tectonophysics* 581, 231-245.
- 556 Lamarche J., 2015a. Facies and Diagenesis Control on Diffuse Fractures in Carbonates. 77th EAGE
557 Conference & Exhibition 2015 Earth Science for Energy and Environment; 1 - 4 June 2015, Madrid
558 Spain.
- 559 Lamarche, J., Lavenu, A., Gauthier B.D.M., 2015b. How far facies and diagenesis control diffuse fractures
560 in carbonates? European Geosciences Union General Assembly 2015; Vienna Austria; 12 – 17 April
561 2015.
- 562 Laubach, S.E., 2003. Practical approaches to identifying sealed and open fractures. *AAPG bulletin*, 87,
563 561-579.
- 564 Laubach, S.E., Eichhubl, P., Hilgers, C., Lander, R.H., 2010. Structural diagenesis. *Journal of Structural*
565 *Geology*, 32, 1866-1872.
- 566 Lavenu, A.P., Lamarche, J., Gallois, A., Gauthier, B.D., 2013. Tectonic versus diagenetic origin of
567 fractures in a naturally fractured carbonate reservoir analog (Nerthe anticline, southeastern
568 France) Tectonic Vs. Diagenetic Fractures in a Naturally Fractured Reservoir. *AAPG bulletin*, 97,
569 2207-2232.
- 570 Lavenu, A.P., Lamarche, J., Salardon, R., Gallois, A., Marié, L., Gauthier, B.D., 2014. Relating background
571 fractures to diagenesis and rock physical properties in a platform–slope transect. Example of the
572 Maiella Mountain (central Italy). *Marine and Petroleum Geology*, 51, 2-19.
- 573 Lavenu, A.P., Lamarche, J., Texier, L., Marié, L., Gauthier, B.D., 2015. Background fractures in
574 carbonates: inference on control of sedimentary facies, diagenesis and petrophysics on rock
575 mechanical behavior. Example of the Murge Plateau (southern Italy). *Italian Journal of*
576 *Geosciences*, 134, 535-555.
- 577 Lavenu, A. P., Lamarche, J., 2018. What controls diffuse fractures in platform carbonates? Insights from
578 Provence (France) and Apulia (Italy). *Journal of Structural Geology*, 108, 94-107.
- 579 Locardi, E., 1988. The origin of the Apennine Arcs. *Tectonophysics* 146, 105-123.

- 580 Lucia, F.J., 2007. Carbonate reservoir characterization: An integrated approach. Springer Science &
581 Business Media.
- 582 Massaro, L., Corradetti, A., Vinci, F., Tavani, S., Iannace, A., Parente, M., Mazzoli S., 2018. Multiscale
583 Fracture Analysis in a Reservoir-Scale Carbonate Platform Exposure (Sorrento Peninsula, Italy):
584 Implications for Fluid Flow,” *Geofluids*, vol. 2018, Article ID 7526425, 10 pages,
585 2018. <https://doi.org/10.1155/2018/7526425>.
- 586 Matonti, C., Guglielmi, Y., Viseur, S., Bruna, P.O., Borgomano, J., Dahl, C., Marié, L., 2015. Heterogeneities
587 and diagenetic control on the spatial distribution of carbonate rocks acoustic properties at the
588 outcrop scale. *Tectonophysics*, 638, 94-111.
- 589 Matonti, C., Guglielmi, Y., Viseur, S., Garambois, S., Marié, L., 2017. P-wave velocity anisotropy related
590 to sealed fractures reactivation tracing the structural diagenesis in
591 carbonates. *Tectonophysics*, 705, 80-92.
- 592 Mazzoli, S., Aldega, L., Corrado, S., Invernizzi, C., Zattin, M., 2006. Pliocene-Quaternary thrusting, syn-
593 orogenic extension and tectonic exhumation in the southern Apennines (Italy): Insights from the
594 Alpi Mt. area. In *Styles of Continental Contraction*, edited by S. Mazzoli and R.W.H. Butler. Geological
595 Society of America 414, 55-77.
- 596 Mazzoli, S., D'errico, M., Aldega, L., Corrado, S., Invernizzi, C., Shiner, P., Zattin, M., 2008. Tectonic burial
597 and “young” (< 10 Ma) exhumation in the southern Apennines fold-and-thrust belt
598 (Italy). *Geology*, 36, 243-246.
- 599 Mazzoli, S., Ascione, A., Buscher, J. T, Pignalosa. A., Valente, E., Zattin, M., 2014. Low-angle normal
600 faulting and focused exhumation associated with late Pliocene change in tectonic style in the
601 southern Apennines (Italy). *Tectonics* 33,1802-1818.
- 602 Meyers, W. J., 1974. Carbonate cement stratigraphy of the Lake Valley Formation (Mississippian)
603 Sacramento Mountains, New Mexico. *Journal of Sedimentary Research*, 44, 837-861.
- 604 Meyers, W.J., 1991. Calcite cement stratigraphy; an overview. *SEPM Short Course Notes*, 25, 133-148.
- 605 Mostardini, F., Merlini, S., 1986. Appennino centro-meridionale. Sezioni geologiche e proposta di
606 modello strutturale. *Memorie della Società Geologica Italiana* 35, 177-202.

- 607 Nelson, R.A., 1981. Significance of fracture sets associated with stylolite zones: geologic notes. AAPG
608 Bulletin, 65, 2417-2425.
- 609 Nelson, R., 2001. Geologic analysis of naturally fractured reservoirs. Elsevier.
- 610 Ortolani, F., Torre, M., 1971. Il Mt. Alpi (Lucania) nella paleogeografia dell'Appennino meridionale.
611 Bollettino della Società Geologica Italiana 90, 213-248.
- 612 Panza, E., Agosta, F., Zambrano, M., Tondi, E., Prosser, G., Giorgioni, M., Janiseck, J. M., 2015. Structural
613 architecture and Discrete Fracture Network modelling of layered fractured carbonates (Altamura
614 Fm., Italy). Italian Journal of Geosciences, 134, 409-422.
- 615 Panza, E., Agosta, F., Rustichelli, A., Zambrano, M., Tondi, E., Prosser, G., Giorgioni, M., Janiseck, J.M.,
616 2016. Fracture stratigraphy and fluid flow properties of shallow-water, tight carbonates: the case
617 study of the Murge Plateau (southern Italy). Marine and Petroleum Geology 73, 350-370.
- 618 Panza, E., Sessa, E., Agosta, F., Giorgioni, M., 2018. Discrete Fracture Network modelling of a
619 hydrocarbon-bearing, oblique-slip fault zone: Inferences on fault-controlled fluid storage and
620 migration properties of carbonate fault damage zones. Marine and Petroleum Geology 89, 263-279.
- 621 Panza, E., Agosta, F., Rustichelli, A., Vinciguerra, S., Ougier-Simonin, A., Dobbs, M. R., Prosser, G., 2019.
622 Meso-to-microscale fracture porosity in tight limestones, results of an integrated field and
623 laboratory study. Marine and Petroleum Geology 103, 581-595.
- 624 Patacca, E., Sartori, R., Scandone, P. 1990. Tyrrhenian basin and Apenninic arcs: kinematic relations
625 since late Tortonian times. Memorie Società Geologica Italiana 45, 425-451.
- 626 Patacca, E., Scandone, P., Bellatalla, M., Perilli, N., Santini, U., 1992. The Numidian-sand event in the
627 Southern Apennines. Mem. Sci. Geol. Padova, 43, 297-337.
- 628 Patacca, E., Scandone, P., 2007. Geology of southern Apennines. Results of the CROP Project. Sub-
629 project CROP-04: In: Mazzotti A., Patacca E., Scandone P., (Eds). Bollettino della Società Geologica
630 Italiana 7, 75-119.
- 631 Petruccio, A. V., Agosta, F., Prosser, G., Rizzo, E., 2017. Cenozoic tectonic evolution of the northern
632 Apulian carbonate platform (southern Italy). Italian Journal of Geosciences 136, 296-311.
- 633 Pieri, P., Festa, V., Moretti, M., Tropeano, M., 1997. Quaternary tectonic activity of the Murge area
634 (Apulian foreland-Southern Italy). Annals of Geophysics 40.

- 635 Richter, D.K., Götze, T., Götze, J., and Neuser, R.D., 2003. Progress in application of
636 cathodoluminescence (CL) in sedimentary petrology. *Mineralogy and Petrology*, 79, 127-166.
- 637 Roda, C., 1965. Livelli a struttura grumosa e livelli ad ooliti rotte e rigenerate nel calcare miocenico del
638 Alpi Mt. (Potenza). *Geologica Romana* 4.
- 639 Royden, L., Patacca, E., Scandone, P., 1987. Segmentation and configuration of subducted lithosphere in
640 Italy: An important control on thrust-belt and foredeep-basin evolution. *Geology*, 15, 714-717.
- 641 Rustichelli, A., Tondi, E., Agosta, F., Cilona, A., Giorgioni, M., 2012. Development and distribution of bed-
642 parallel compaction bands and pressure solution seams in carbonates (Bolognaro Formation,
643 Majella Mountain, Italy). *Journal of Structural Geology*, 37, 181-199
- 644 Rustichelli, A., Agosta, F., Tondi, E., Spina, V., 2013. Spacing and distribution of bed perpendicular joints
645 throughout layered, shallow-marine carbonates (Granada Basin, southern Spain). *Tectonophysics*
646 582, 188-204.
- 647 Rustichelli, A., Tondi, E., Korneva, I., Baud, P., Vinciguerra, S., Agosta, F., Reuschlé, T., Janiseck, J.M.,
648 2015. Bedding-parallel stylolites in shallow-water limestone successions of the Apulian Carbonate
649 Platform (central-southern Italy). *Italian Journal of Geosciences*, 134, 513-534.
- 650 Rustichelli, A., Torrieri, S., Tondi, E., Laurita, S., Strauss, C., Agosta, F., Balsamo, F., 2016. Fracture
651 characteristics in Cretaceous platform and ramp carbonates: an outcrop study from Maiella
652 Mountain (central Italy). *Marine and Petroleum Geology* 76, 68-87.
- 653 Sartoni, S., Crescenti U., 1962. Ricerche biostratigrafiche nel Mesozoico dell'Appennino Meridionale.
654 *Giornale di Geologia* 29, 161-309.
- 655 Selli, R., 1957. Sulla trasgressione del Miocene nell'Italia meridionale. *Giornale Di Geologia* 2, 26-54.
- 656 Shiner, P., Beccacini, A., Mazzoli, S., 2004. Thin-skinned versus thick-skinned structural models for
657 Apulian Carbonate Reservoirs: constraints from the Val D'Agri Field. *Marine and Petroleum Geology*
658 21, 805-827.
- 659 Sgrosso, I., 1988. Nuovi dati biostratigrafici sul Miocene del M. Alpi (Lucania) e conseguenti ipotesi
660 paleogeografiche. *Memorie della Società Geologica Italiana* 41, 343-351.


- 661 Spalluto, L., 2012. Facies evolution and sequence chronostratigraphy of a “mid”-Cretaceous shallow-
662 water carbonate succession of the Apulia Carbonate Platform from the northern Murge area
663 (Apulia, southern Italy). *Facies* 58, 17-36.
- 664 Strasser, A., Pittet, B., Hillgärtner, H., Pasquier, J.B., 1999. Depositional sequences in shallow carbonate-
665 dominated sedimentary systems: concepts for a high-resolution analysis. *Sedimentary Geology*, 128,
666 201-221.
- 667 Taddei, A., Siano, M. G., 1992. Analisi biostratigrafica e considerazioni paleoecologiche sulla
668 successione neogenica del Alpi Mt. (Lucania). *Bollettino della Società Geologica Italiana* 111, 255-
669 272.
- 670 Tavani, S., Storti, F., Lacombe, O., Corradetti, A., Muñoz, J. A. Mazzoli, S., 2015. A review of deformation
671 pattern templates in foreland basin systems and fold-and-thrust belts: Implications for the state of
672 stress in the frontal regions of thrust wedges. *Earth Sciences Reviews* 141, 82-104.
- 673 Tavani, S., Vitale, S., Grifa, C., Iannace, A., Parente, M., Mazzoli, S. 2016. Introducing dolomite seams:
674 hybrid compaction–solution bands in dolomitic limestones. *Terra Nova*, 28, 195-201.
- 675 Tucker, M.E., Wright, V.P., 1990. *Carbonate sedimentology*. John Wiley & Sons.
- 676 Warren, J.E, Root, P.J., 1963. The behavior of Naturally Fractured Reservoirs. *SPE journal* 426, 245-255.
- 677 Wennberg, O.P., Svana, T., Azizzadeh, M., Aqrawi, A.M.M., Brockbank, P., Lyslo, K.B., Ogilvie, S., 2006.
678 Fracture intensity vs. mechanical stratigraphy in platform top carbonates: the Aquitanian of the
679 Asmari Formation, Khaviz Anticline, Zagros, SW Iran. *Petroleum Geoscience*, 12, 235-246.
- 680 Vai, G.B., Martini, I. P., 2001. Basement and early (pre-Alpine) history. In Vai, G. B., Martini, I. P., Eds.,
681 *Anatomy of an Orogen: The Apennines and Adjacent Mediterranean Basins*. Kluwer Academic
682 Publication 121-150.
- 683 Van Dijk, J. P., Bello, M., Toscano, C., Bersani, A., Nardon, S., 2000. Tectonic model and three-
684 dimensional fracture network analysis of Alpi Mt. (southern Apennines). *Tectonophysics* 324, 203-
685 237.
- 686 Vinci, F., Iannace, A., Parente, M., Pirmez, C., Torrieri, S., Giorgioni, M., 2017. Early dolomitization in the
687 Lower Cretaceous shallow-water carbonates of Southern Apennines (Italy): Clues about
688 palaeoclimatic fluctuations in western Tethys. *Sedimentary geology*, 362, 17-36.

689 Vitale, S., Dati, F., Mazzoli, S., Ciarcia, S., Guerriero, V., Iannace, A., 2012. Modes and timing of fracture
 690 network development in poly-deformed carbonate reservoir analogues, Mt. Chianello, southern
 691 Italy. *Journal of Structural Geology*, 37, 223-235.

692 Vitale, S., Ciarcia, S., 2013. Tectono-stratigraphic and kinematic evolution of the southern
 693 Apennines/Calabria–Peloritani Terrane system (Italy). *Tectonophysics*, 583, 164-182.

694

695 **Figure captions**

696 **Fig.1.** (a) Simplified geological map of Southern Apennines, Italy (from Bonardi et al., 1988; Cosentino
 697 et al., 2003; Patacca and Scandone 2007; Vitale and Ciarcia, 2013,) and NE-SW geological cross-section
 698 modified after Mazzoli et al., 2008. (b) Sketch map of part of the southern Apennines showing the
 699 study area. 

700

701 **Fig.2.** Geological map of Monte Alpi, (Basilicata, Italy; modified after La Bruna et al., 2017) with
 702 location of the studied sites.

703

704 **Fig.3.** (a) Panoramic overview of the western edge of Monte Alpi; (b) focus on the southern portion of
 705 the western cliff; (c) stratigraphic log; (d) outcrop view of the studied Solarino site; (e) close up view
 706 of the studied outcrop; (f) line drawing of the studied outcrop; (g) lower hemisphere equal area
 707 projection of the structures presented in e.

708

709 **Fig.4.** (a) Close up view of the southern portion of the western cliff; (b) panoramic overview of the
 710 Monte Teduro cliff; (c) close up of a portion of the studied Monte Teduro cliff; (d) stratigraphic log; (e)
 711 view of the studied outcrop; (f) close up of the outcrop; (g) line drawing map of the studied outcrop;
 712 (h) lower hemisphere equal area projection of the structures presented in g.

713

714 **Fig.5.** (a to d) Photomicrographs (cross-polarized light) of representative microfacies of the Lower
 715 Cretaceous platform carbonates.

716

717 **Fig.6.** Solarino site, (a) Scanned thin-section; (b) line drawing of the scanned thin-section; (c) cartoon
 718 of the structural assemblage presented in b; (d) lower hemisphere equal area projection as poles of
 719 the structures that are presented in b and c.

720

721 **Fig.7.** Thin-section zooms a to e: planar-polarized light and cathodoluminescence microphotographs
 722 showing the main characteristics and chronologies of fractures and cements. See text for explanation.

723

724 **Fig.8.** Teduro site, (a) Scanned thin section; (b) line drawing of the scanned thin section; (c) cartoon of
 725 the structural assemblage documented in b; (d) lower hemisphere equal area projection as poles of
 726 the structures presented in b and c.

727

728 **Fig.9.** Thin section focus a to d natural light and cathodoluminescence microphotographs of the
 729 showing the main characteristics and chronologies of fractures and cements. See text for explanation.

730

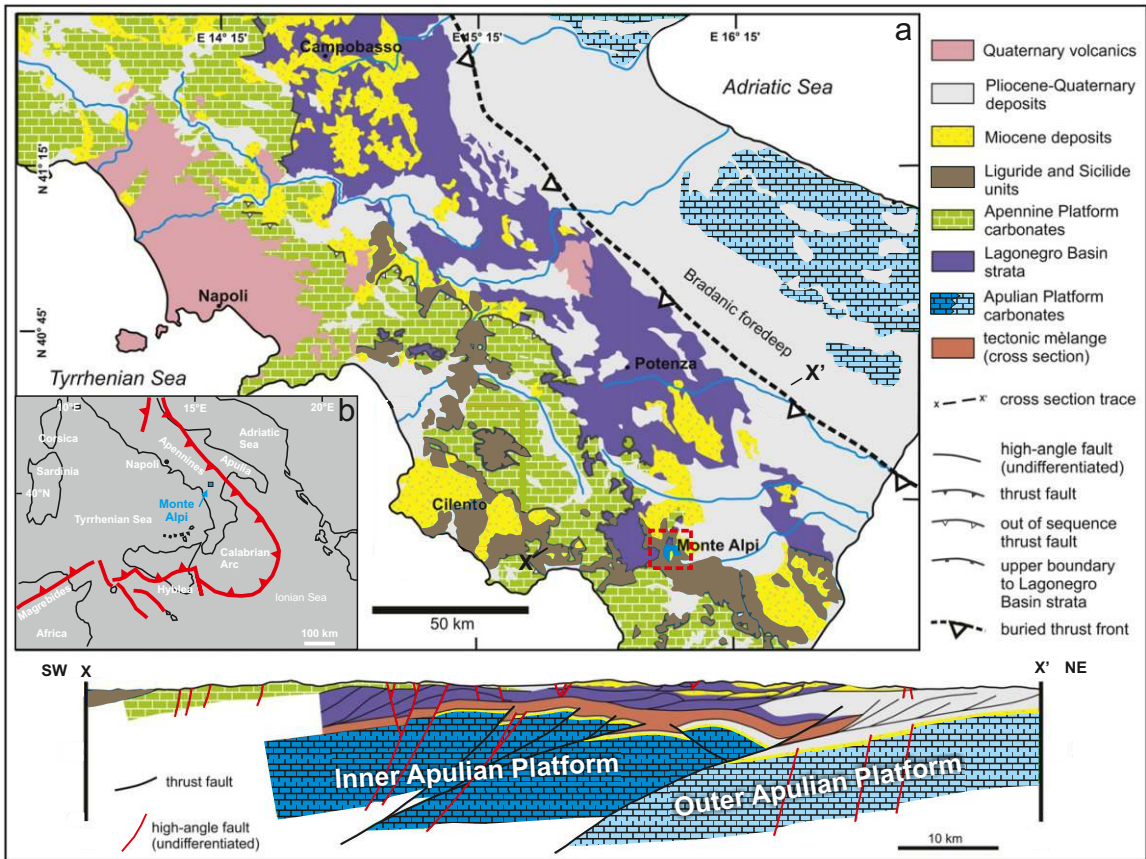
731 **Fig.10.** Scanned image of a *Lithoclastic-oncolitic floatstone*. Plane-polarized light and
732 cathodoluminescence photomicrographs (zoom 1) display early calcite cement localized within bores.
733 Bores formed after blocky cement which filled previous cavities. Cavities are related to a platform
734 emersion phase, differently bores formed during subsequent marine transgression and were filled
735 with early calcite cement (ec).
736

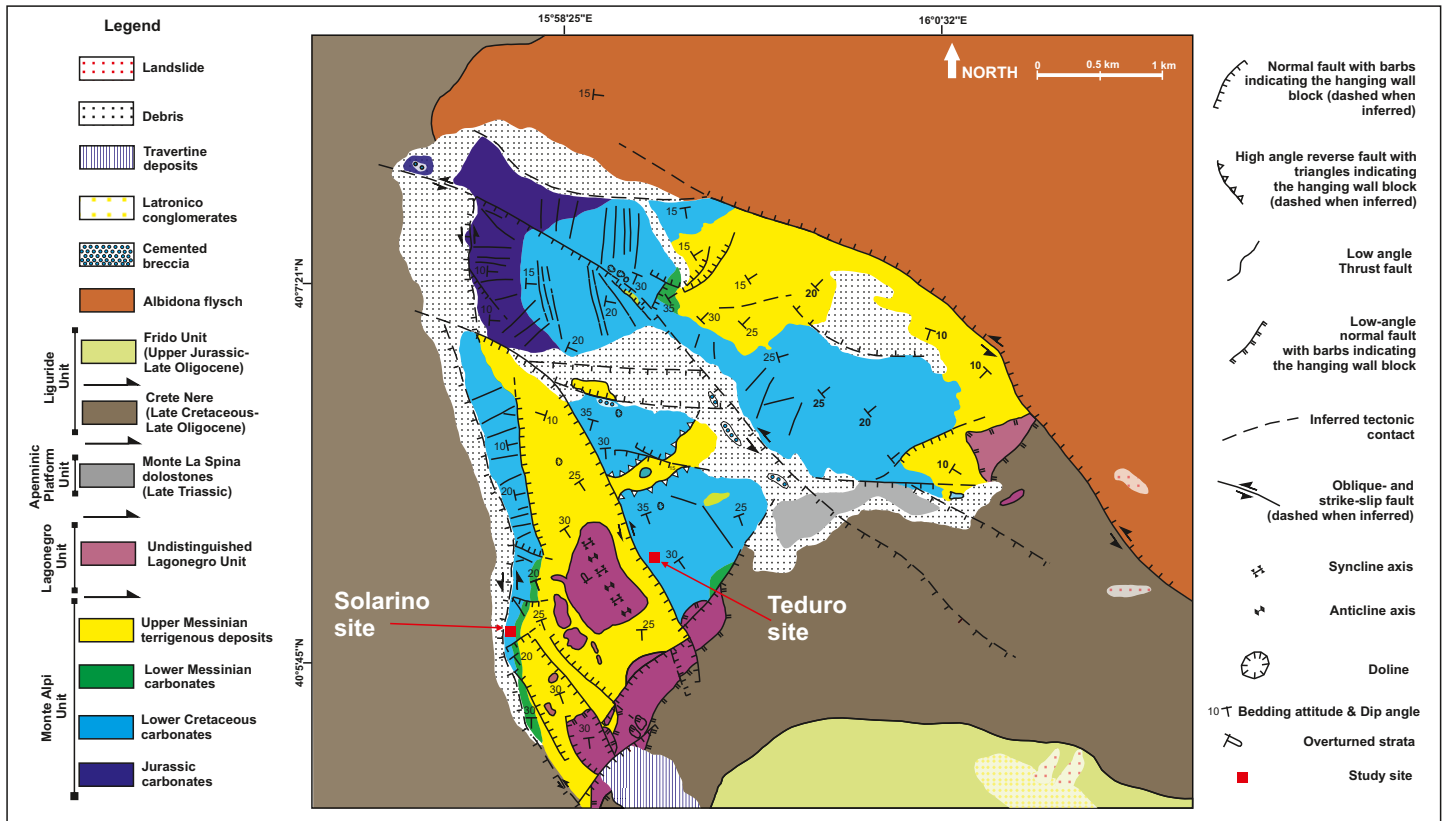
737 **Fig.11.** Scanned image of *Fenestral microbial bindstone*. Early calcite cement filled geopetal
738 structures. Plane-polarized and cathodoluminescence photomicrographs (zoom 1 and 2) display large
739 patches of blocky calcite cement and geopetal early features which represent a typical early diagenetic
740 fabric.
741

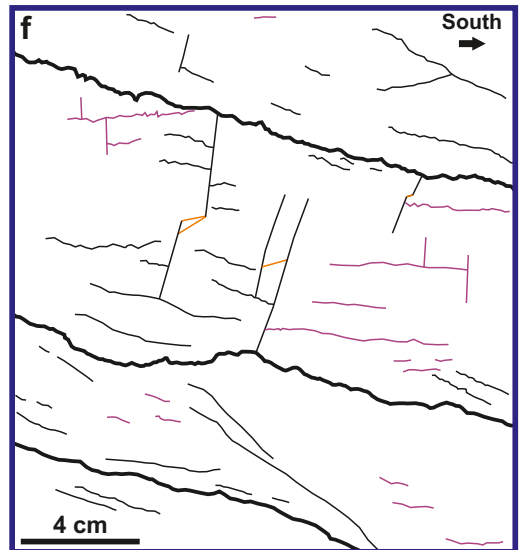
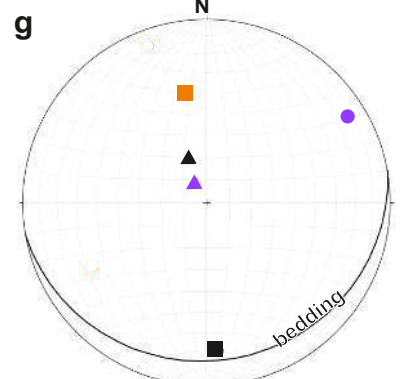
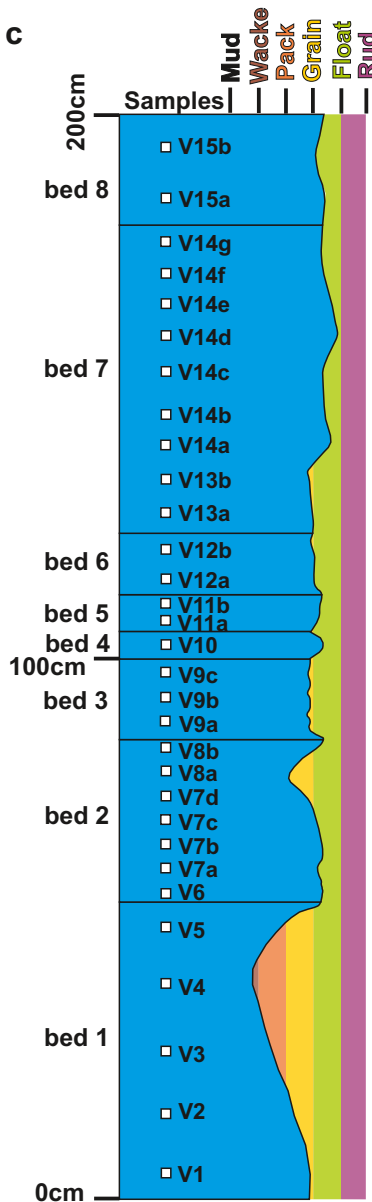
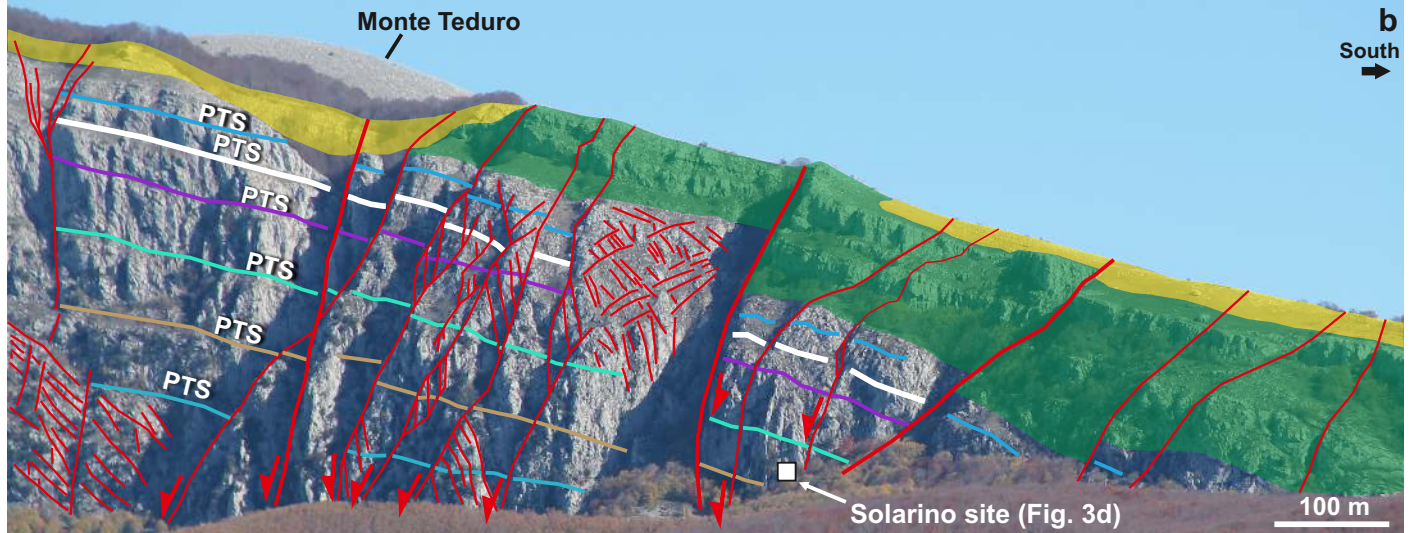
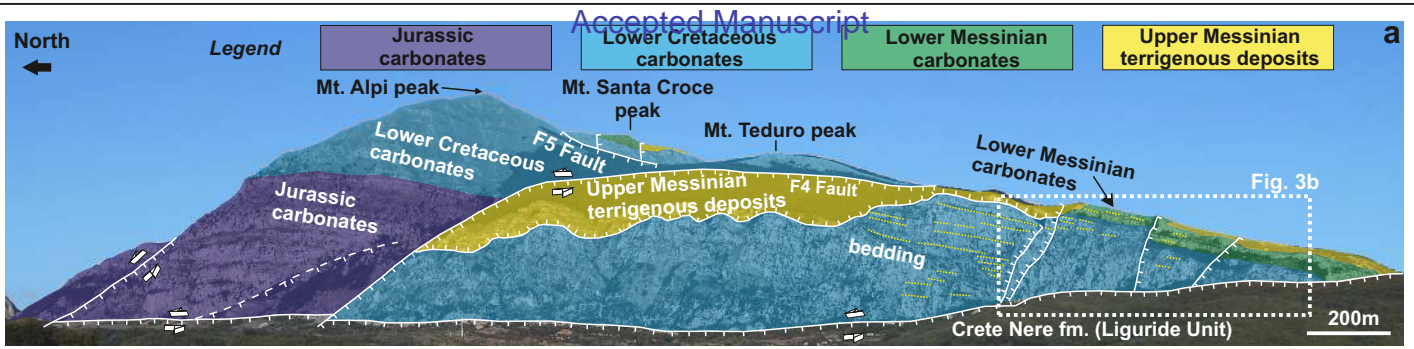
742 **Fig.12.** Diagenetic/structural processes and sequence for the Lower Cretaceous limestone rocks.
743 Bottom: conceptual evolution model of the structural elements crosscutting the Lower Cretaceous
744 carbonates.
745

746 **Fig.13.** Time/space evolution model proposed for Monte Alpi. **(a)** main tectonic steps from the pre-
747 Messinian to the Holocene time (after La Bruna et al, 2017-2018); **(b)** burial history of the Monte Alpi
748 Apulian carbonates associated to the main tectonic events presented in **a** (modified after Mazzoli et al.,
749 2006); **(c)** idealized block diagrams showing the overall structural assemblages observed at meso and
750 microscale.
751

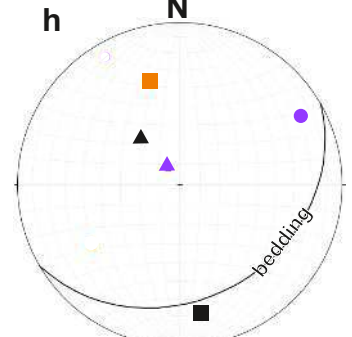
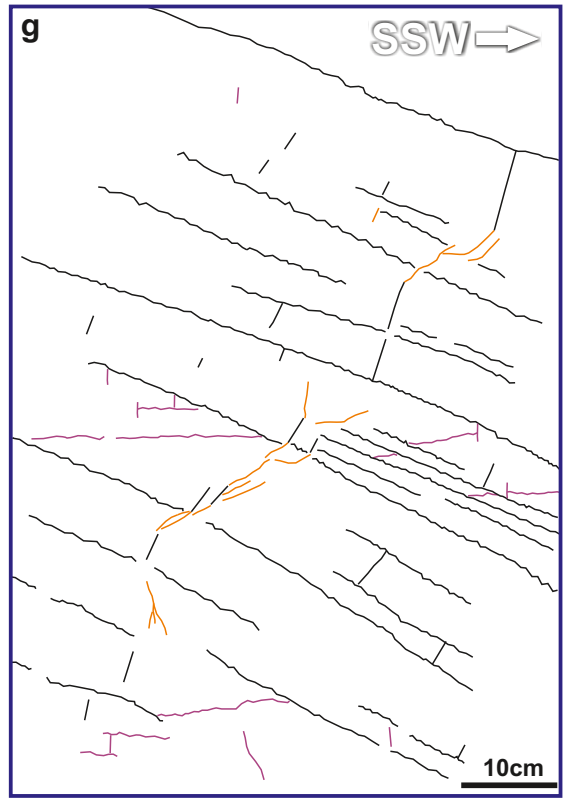
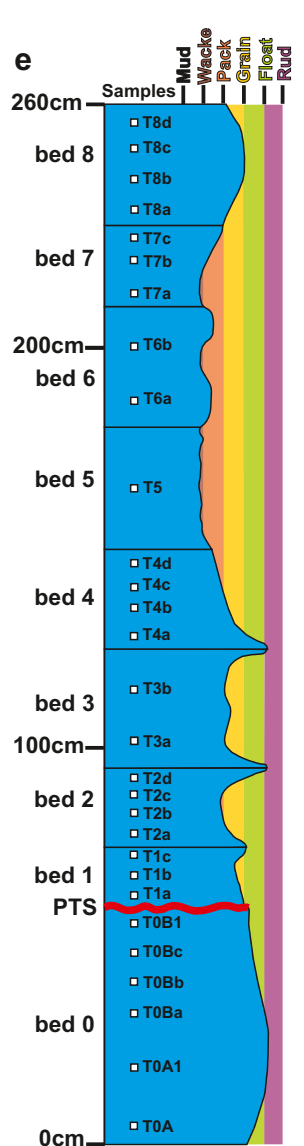
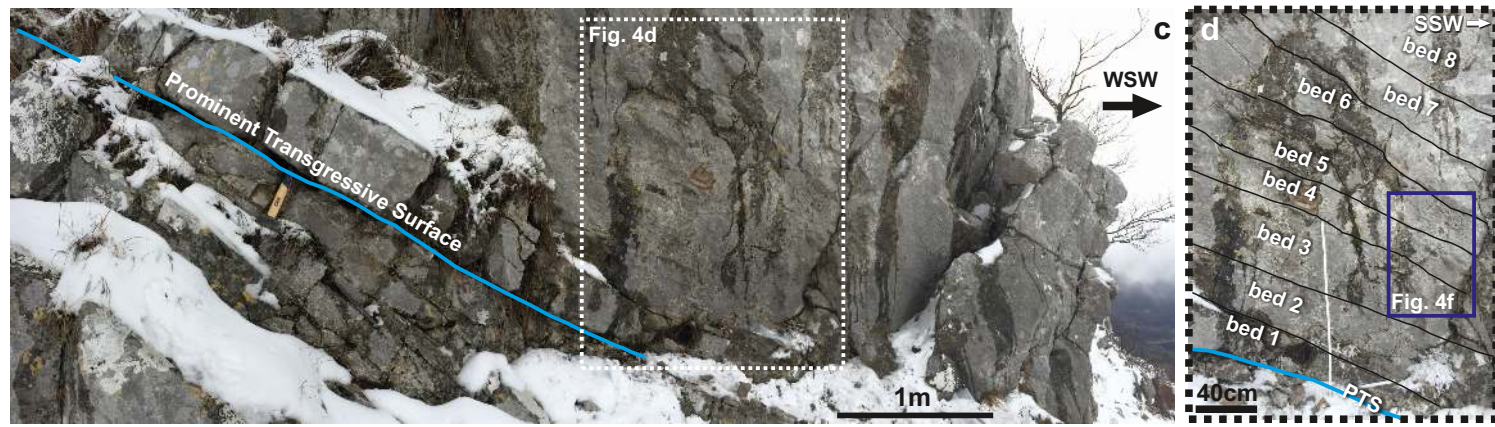
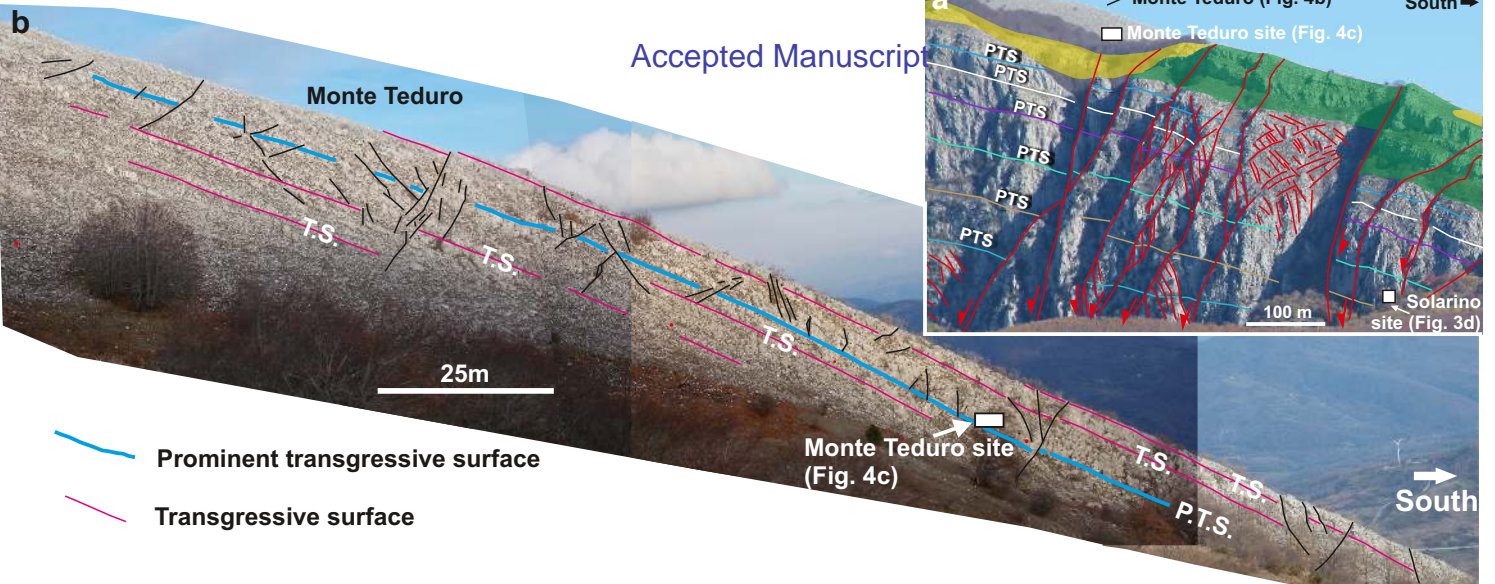
752 **Table1** and **2** display the sedimentological and diagenetic characteristics of the studied rock samples.



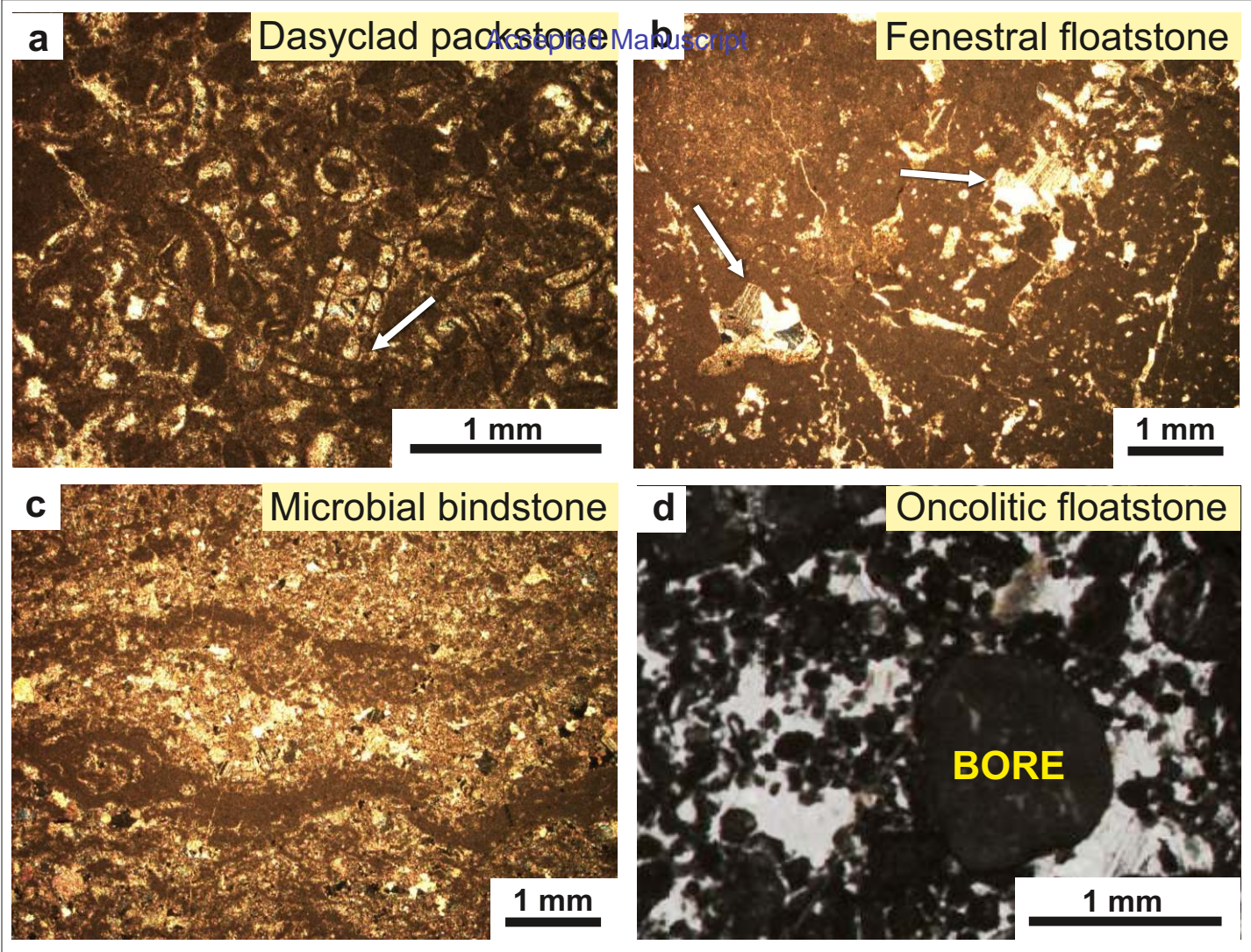


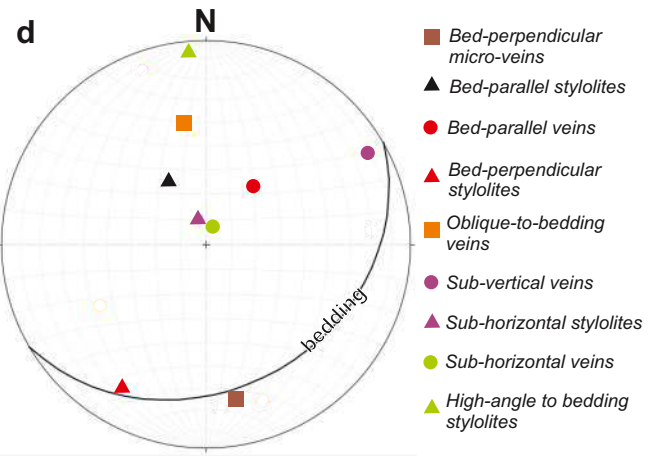
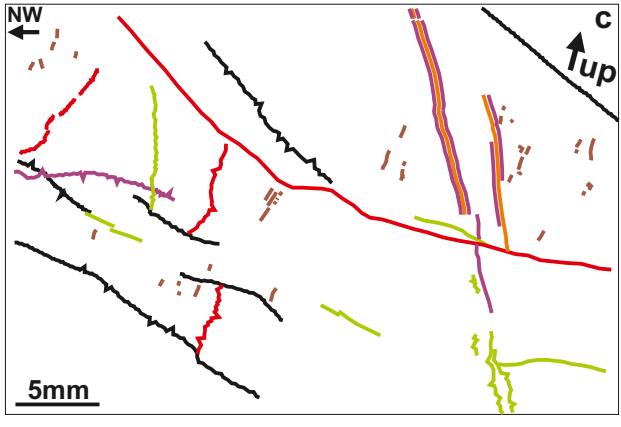
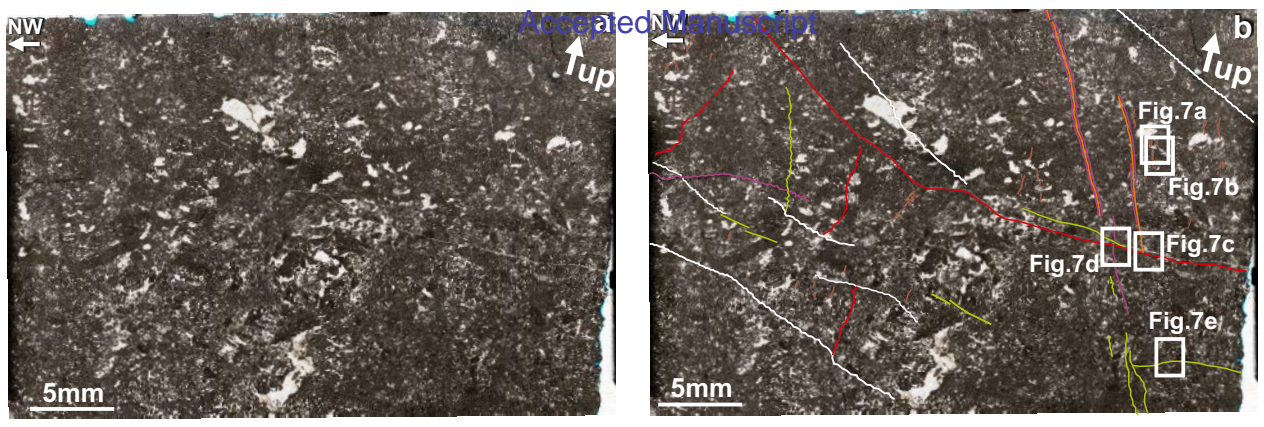


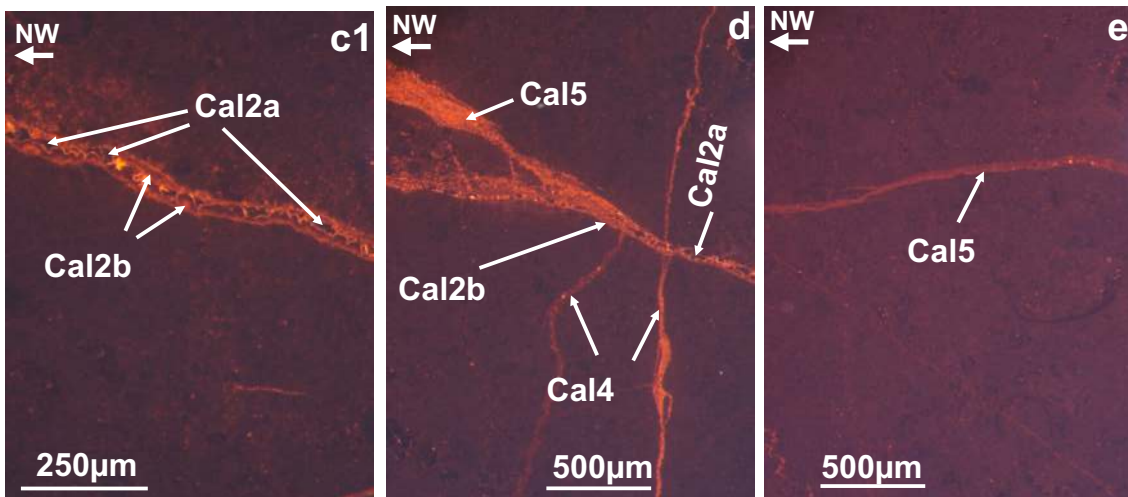
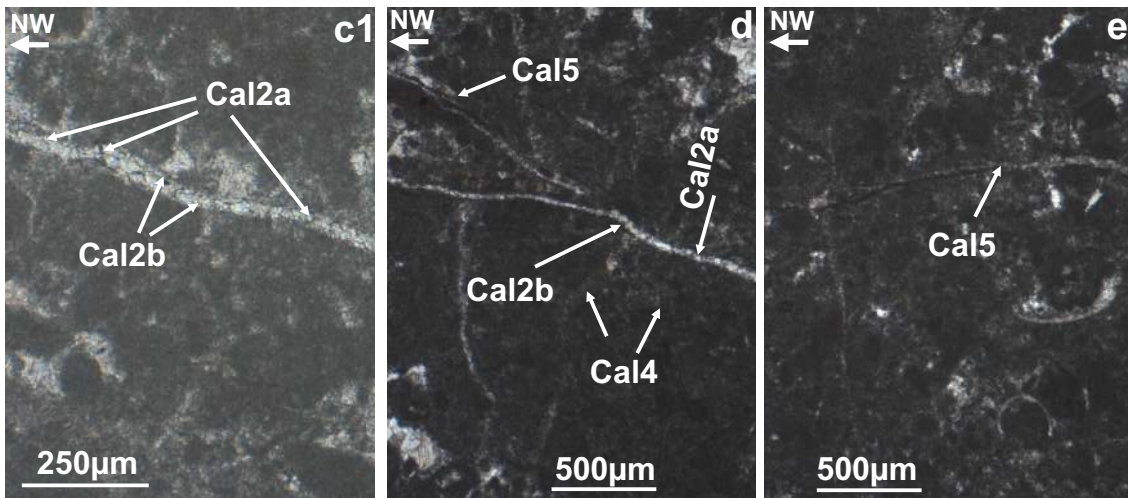
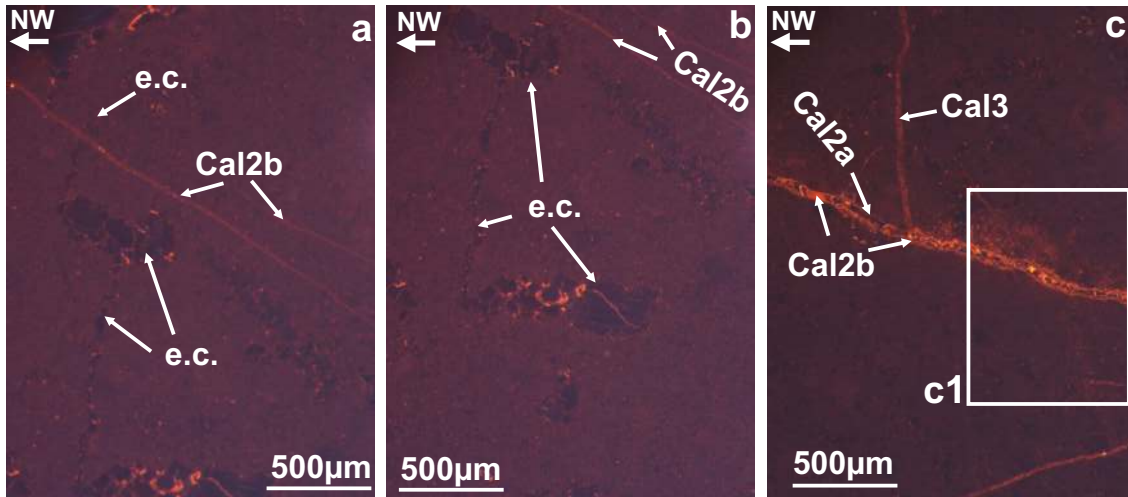
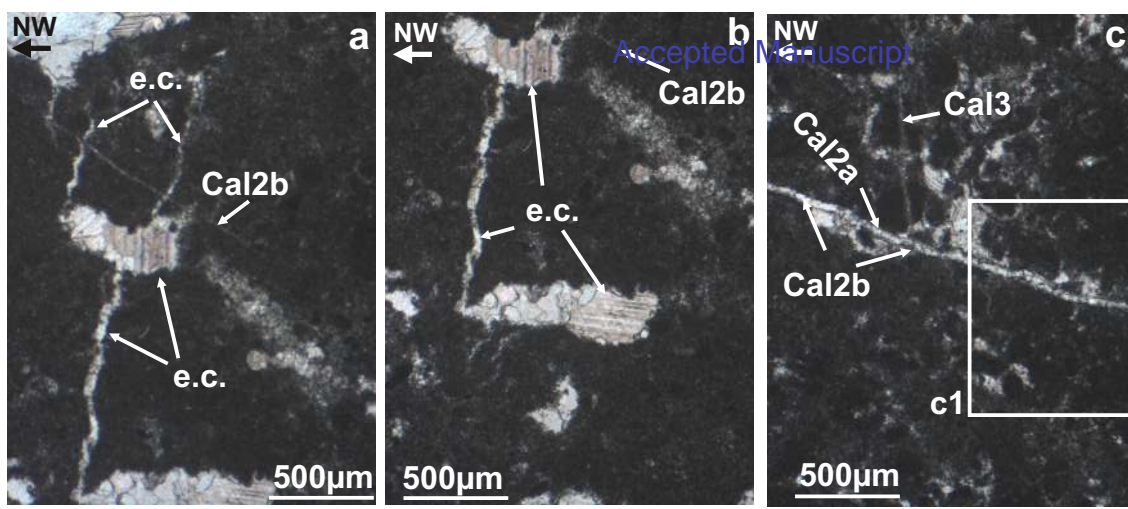
- Bed-perpendicular joints /
- ▲ Bed-parallel stylolites ~~~~~
- Oblique-to-bedding joints |
- Sub-vertical joints |
- ▲ Sub-horizontal stylolites ~~~~~

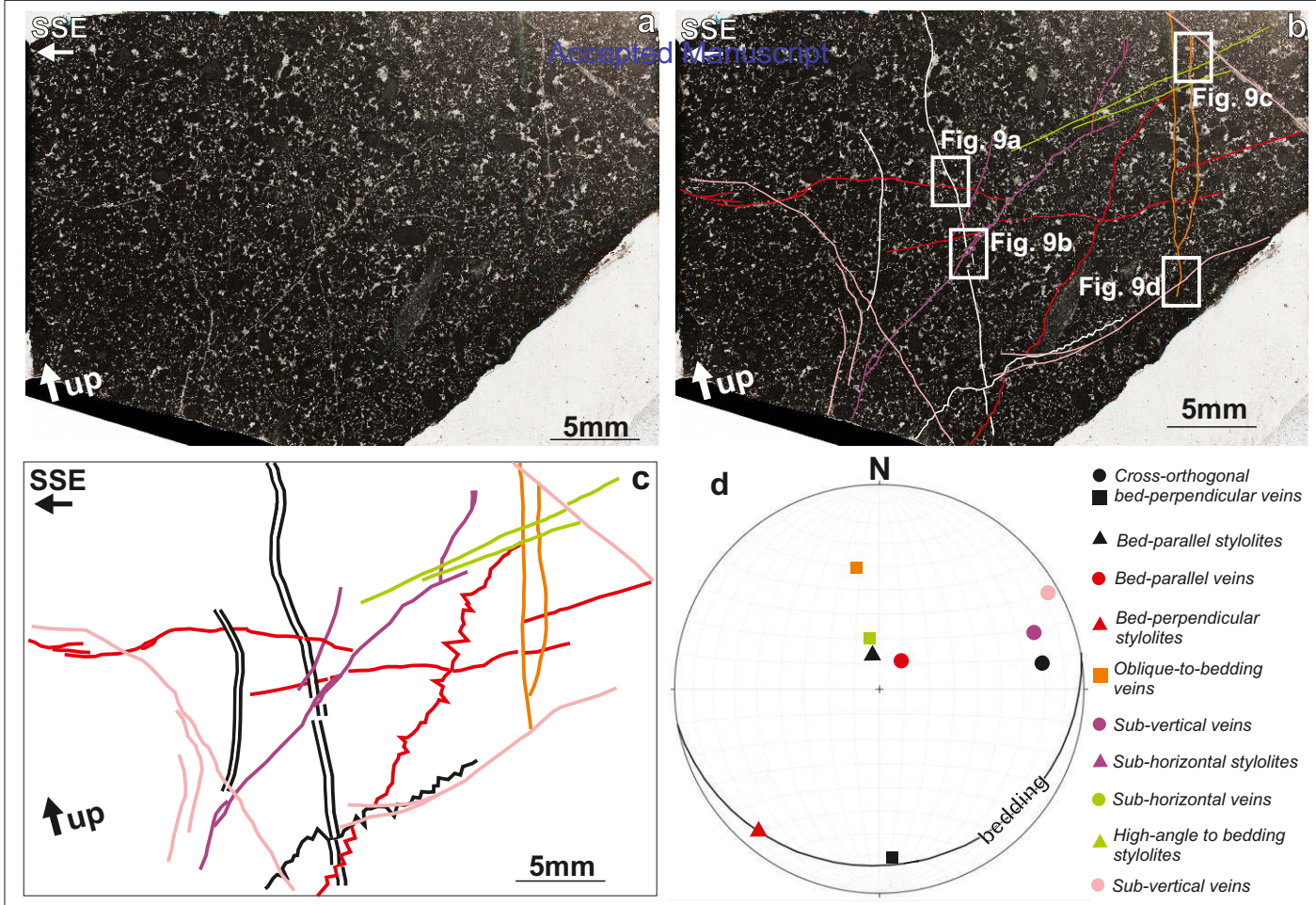


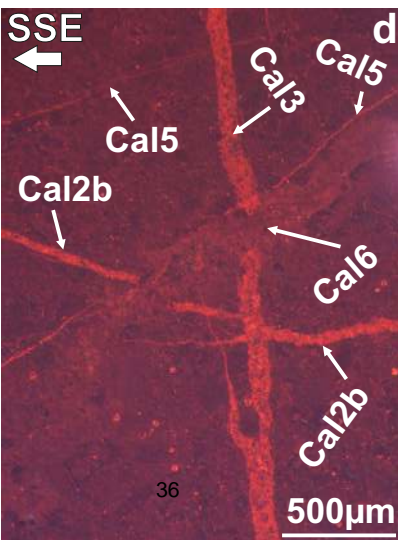
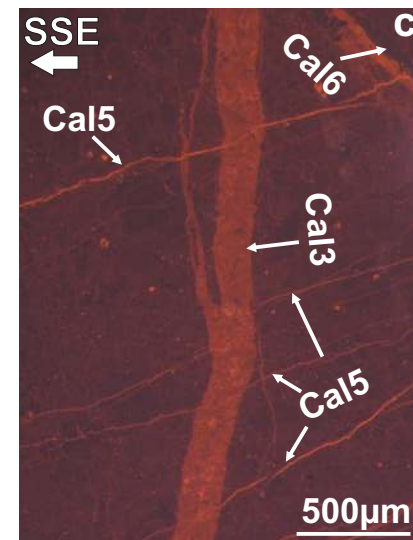
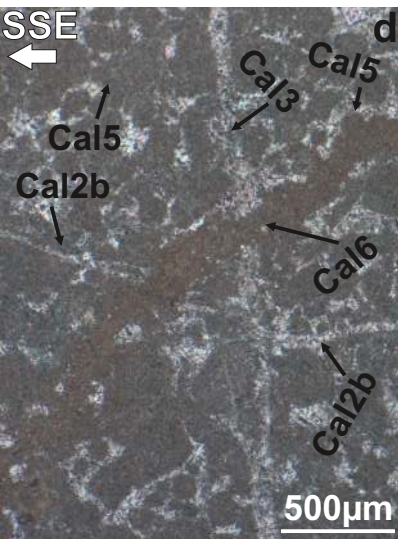
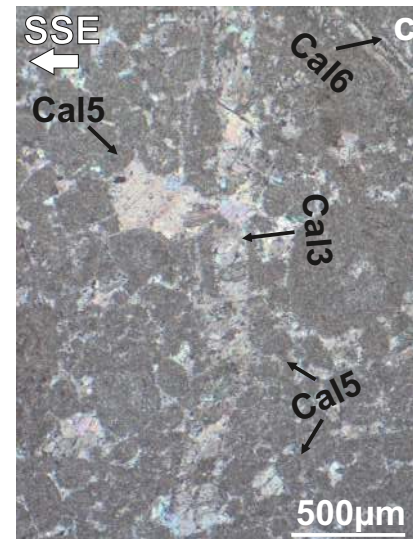
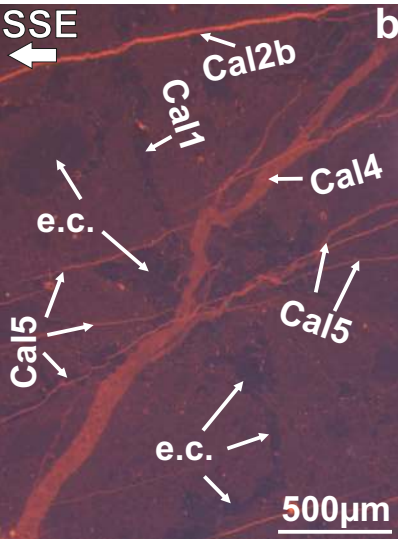
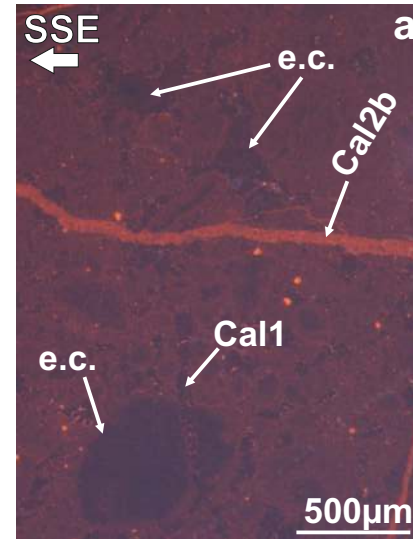
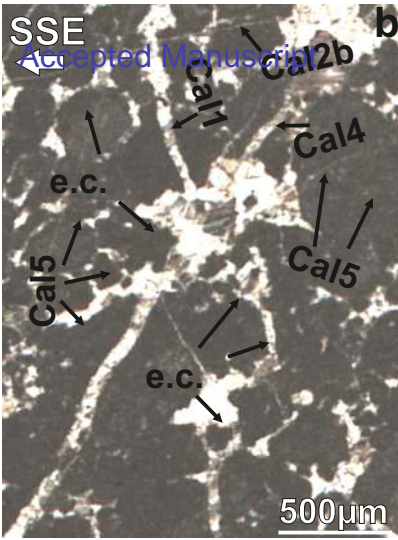
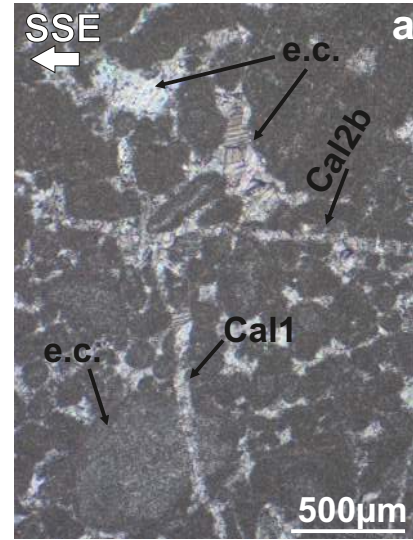
- Bed-perpendicular joints /
- ▲ Bed-parallel stylolites
- Oblique-to-bedding joints |
- Sub-vertical joints |
- ▲ Sub-horizontal stylolites

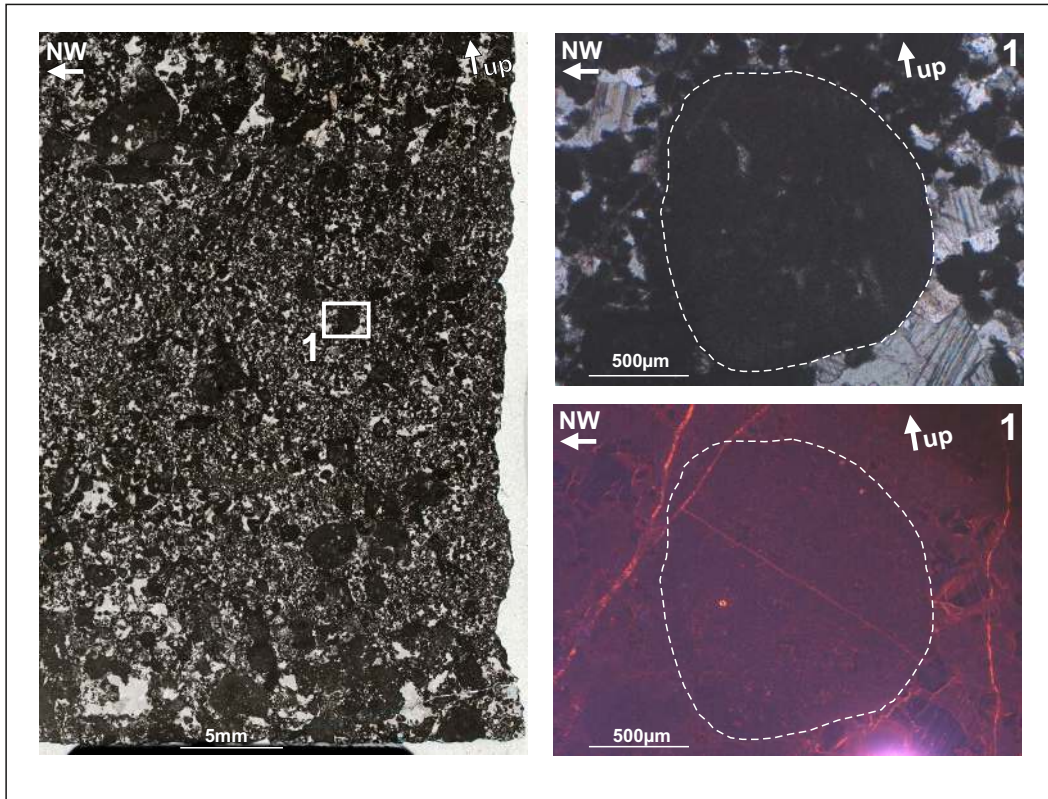


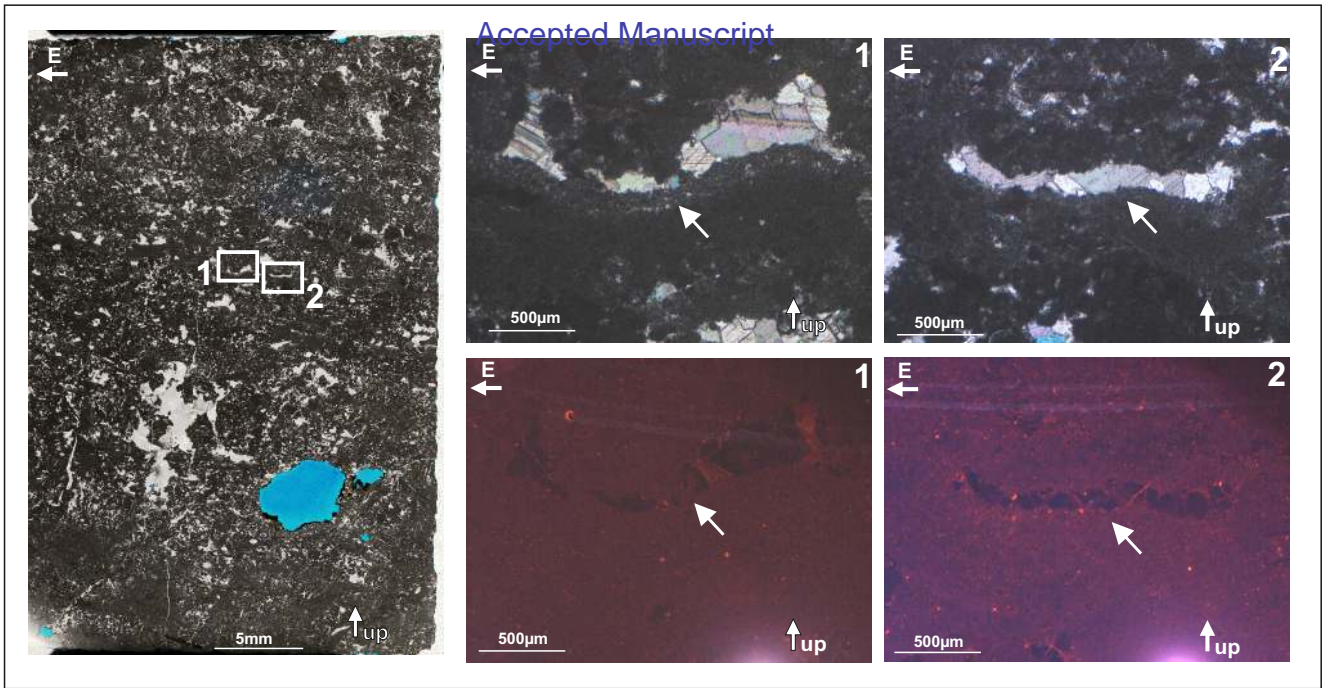


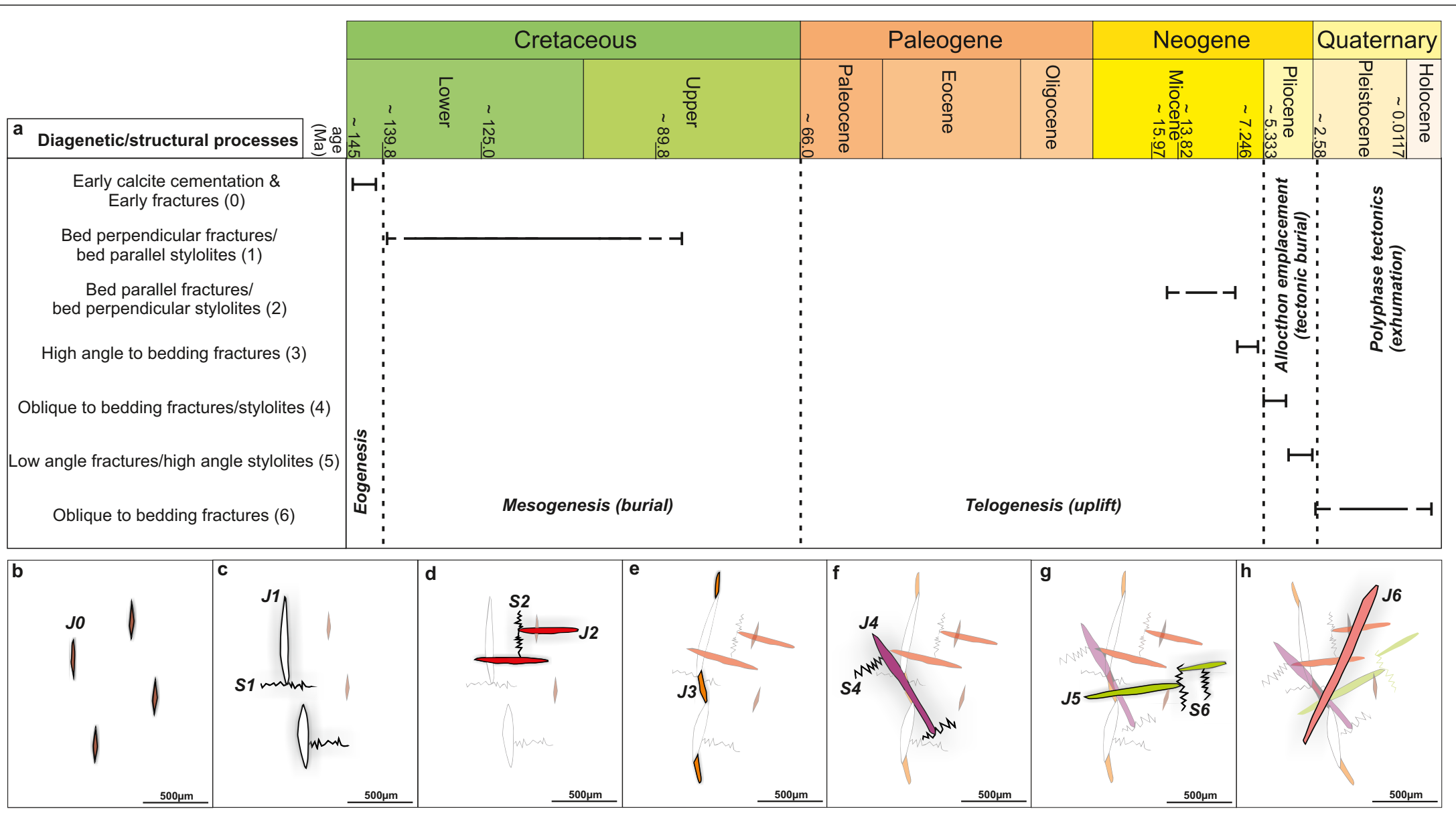


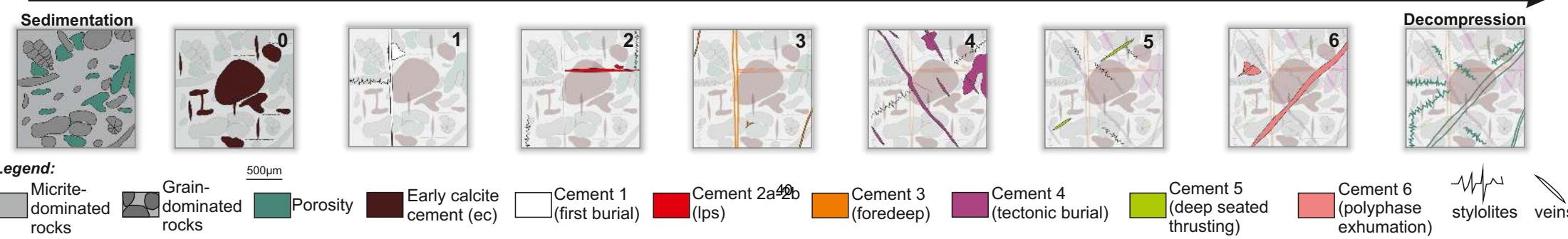
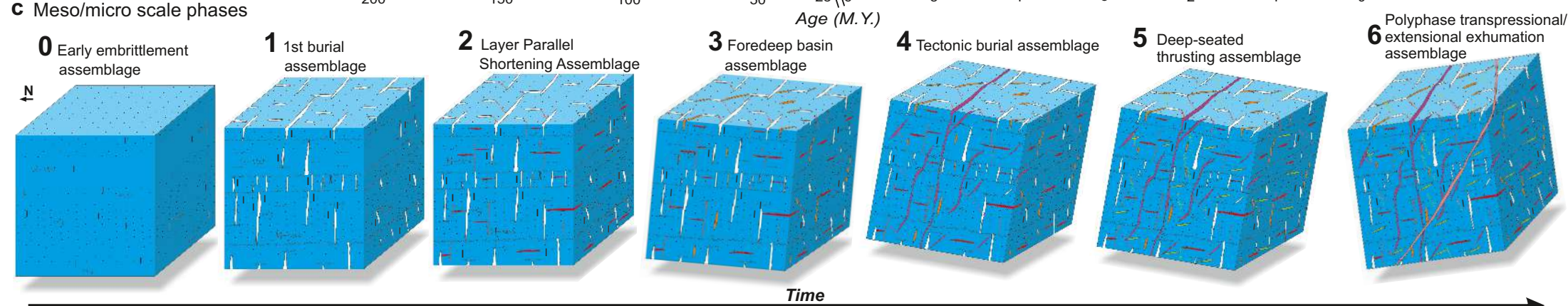
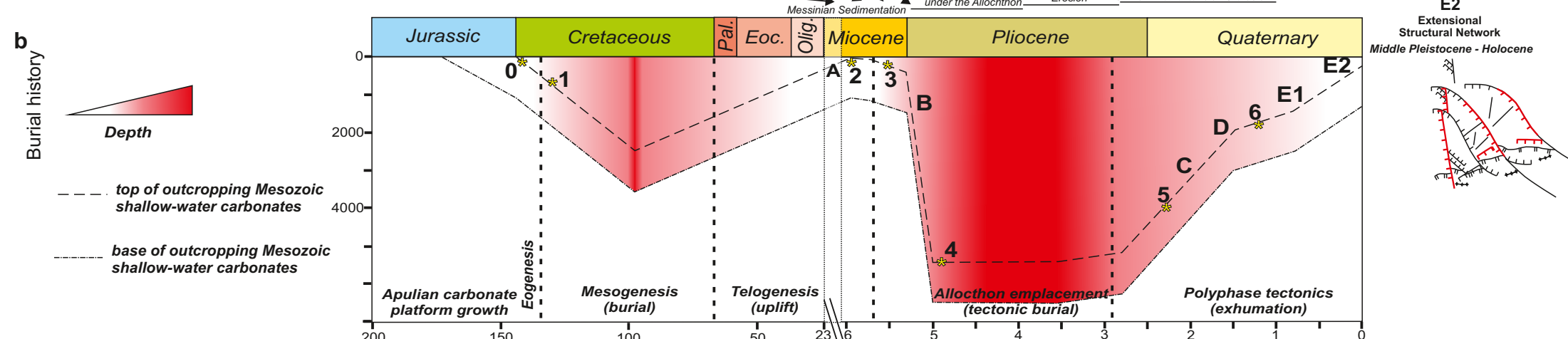
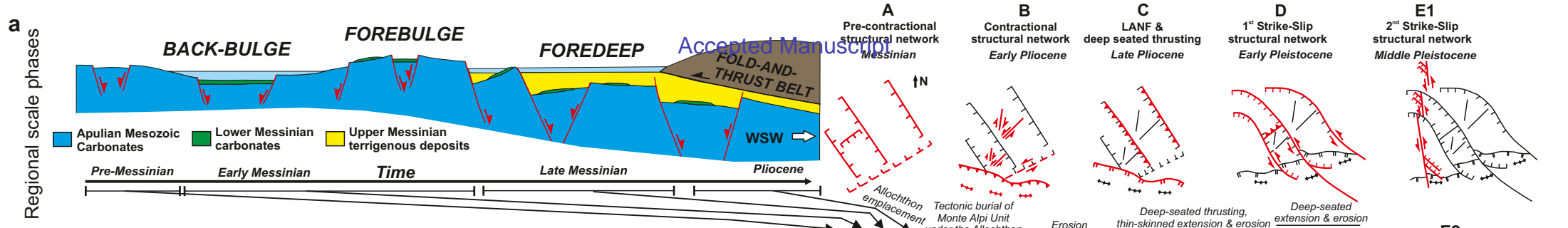












Bed	Sample code	Thin section code	Microfacies name	Biota and allochems	Sedimentary and biogenic structures	Diagenetic products
1	V1	V1	Oncolitic grainstone-packstone-floatstone	O BF Bb		D
1	V2	V2	Oncolitic grainstone-packstone-floatstone	O BF Bb		D
1	V3	V3	Oncolitic grainstone-packstone	O BF Bb		D
1	V4	V4	Green-algal wackestone-packstone	GA Os BF		BC
1	V5	V5	Fenestral microbial bindstone	O Bb GA Os	SL FF	
2	V6	V6	Oncolitic grainstone-packstone-floatstone	O Bb Os BF		
2	V7A	V7a	Fenestral microbial bindstone	Os O Bb GA	SL FF	
2	V7A	V7b	Oncolitic grainstone-packstone-floatstone	O Os		
2	V7B	V7c	Oncolitic grainstone-packstone-floatstone	O Os G		
2	V7B	V7d	Oncoidal-skeletal grainstone	O Bb Os		BC
2	V8strike	V8a	Oncolitic-skeletal grainstone-packstone-floatstone	O Os BF		BC
2	V8strike	V8b	Oncolitic-skeletal grainstone-packstone-wackestone	O Os Bb		BC
2	V8dip	V8c	Oncolitic-skeletal grainstone-packstone-floatstone	O Bb Os		BC
3	V9	V9a	Oncolitic-skeletal grainstone-packstone-floatstone	O Bb Os		BC
3	V9	V9b	Oncolitic-skeletal grainstone-packstone-floatstone	O Bb Os		
3	V9	V9c	Oncolitic-skeletal grainstone-packstone-floatstone	O Bb GA Os BF		BC
4	V10	V10	Oncolitic grainstone-floatstone	O		
5	V11A	V11a	Fenestral microbial bindstone	O Os G	FF SL	
5	V11B	V11b	Fenestral oncolitic grainstone-floatstone	O Os	FF	
6	V12	V12a	Microbial bindstone	O Os	SL FF	
6	V12	V12b	Fenestral microbial bindstone	O Os Bb GA	SL FF	
7	V13A	V13a	Oncolitic grainstone- packstone	O G GA		BC GS
7	V13B	V13b	Oncolitic grainstone- packstone	O G GA		BC GS
7	V14	V14a	Oncolitic grainstone- packstone	O G GA Os		BC GS
7	V14	V14b	Oncolitic grainstone-packstone-floatstone	O Bb G GA		BC GS
7	V14	V14c	Oncolitic grainstone-floatstone	O BF Os		BC GS
7	V14	V14d	Oncolitic grainstone-floatstone	O G GA Os		BC GS
7	V14	V14e	Oncolitic-skeletal floatstone	O G GA Os		BC GS
7	V14	V14f	Oncolitic-skeletal grainstone-floatstone	O G GA Os		BC GS
7	V14	V14g	Oncolitic-skeletal grainstone-floatstone	O G GA Os		BC GS
7	V15	V15a	Oncolitic-skeletal grainstone-floatstone-packstone	O BF GA Os		BC
7	V15	V15b	Oncolitic-skeletal grainstone-floatstone-packstone	O BF G GA Os		BC GS

Biota and allochems (dominant - minor components)

O = oncooids

BF = benthic foraminifera

Bb = bivalve bioclasts

GA = dasycladacean green algae fragments

Os = ostracods (disarticulated valves)

Sedimentary - biogenic structures (dominant - minor components)

SL = bed-parallel stromatolitic laminae

FF = cement-filled fenestral features

Diagenetic products (dominant - minor components)

D = sparse crystals of euhedral dolomite

BC = large patches of blocky calcite cement

Bed	Sample code	Thin section code	Microfacies name	Biota and allochems	Sedimentary and biogenic structures	Diagenetic products
0 PTS	T0A	T0A	Oncolitic grainstone-packstone	O GA Os		BC
0 PTS	T0A1	T0A1	Oncolitic grainstone-floatstone	O GA Os G	Bu Bo	
0 PTS	T0B	T0Ba	Lithoclastic-oncolitic floatstone	O L BF Bb Os G	Bo	BC
0 PTS	T0B	T0Bb	Lithoclastic-oncolitic floatstone	O L BF OS G	Bo	BC
0 PTS	T0B	T0Bc	Lithoclastic-oncolitic floatstone	O L Os G		BC
0 PTS	T0B1	T0B1	Fenestral oncolitic floatstone	O G	FF	
1	T1dip	T1a	Bioturbated grainstone-floatstone	Os G	Bu Bo	
1	T1dip	T1b	Burrowed, fenestral grainstone-packstone	O BF	FF Bu	BC GS
1	T1dip	T1c	Burrowed, fenestral grainstone-packstone	O BF Os	FF Bu	BC GS
1	T1strike	T1d	Fenestral microbial bindstone	O Os P	Bu Bo FF SL	BC V GS
1	T1strike	T1e	Fenestral microbial bindstone	Os P O	SL FF	
1	T1strike	T1f	Fenestral microbial bindstone	Os P O	SL FF	
2	T2A	T2a	Bioturbated bioclastic packstone-wackestone	BF Os G	Bu Bo	
2	T2B	T2b	Burrowed bioclastic packstone-wackestone	BF Bb Os G	Bu	
2	T2B	T2c	Gastropod floatstone (with wackestone matrix)	BF Bb Os G	Bu	
2	T2B	T2d	Burrowed bioclastic packstone-wackestone	BF Bb Os G	Bu	
3	T3	T3a	Burrowed packstone	BF Bb Os P	Bu	
3	T3	T3b	Bioclastic packstone	BF Bb Os P G		
4	T4A	T4a	Bioclastic floatstone (with packstone matrix)	BF Bb Os O P	Bu Bo	
4	T4B	T4b	Bioclastic packstone	BF Bb Os G P	Bu Bo	
4	T4C	T4c	Bioturbated bioclastic packstone-wackestone	BF Bb Os G	Bu Bo	BC
4	T4C	T4d	Bioclastic packstone-wackestone	BF Bb Os G P	Bu Bo	
5	T5	T5	Burrowed bioclastic packstone-wackestone	BF Bb Os G P	Bu	
6	T6	T6a	Bioturbated bioclastic wackestone-packstone	BF Os O P	Bu Bo	BC
6	T6	T6b	Burrowed bioclastic wackestone-packstone	BF Bb GA Os G	Bu	BC V
7	T7A	T7a	Bioturbated bioclastic wackestone-packstone	Os P	Bu Bo	BC
7	T7B	T7b	Bioturbated bioclastic wackestone-packstone	BF Os	Bu Bo	BC
7	T7B	T7c	Bioturbated bioclastic packstone	Bb GA	Bu Bo	
8	T8	T8a	Bioturbated bioclastic packstone	Bb Os	Bu Bo	BC
8	T8	T8b	Bioturbated bioclastic-oncolitic grainstone-packstone	BF Os O	Bu Bo FF	BC
8	T8	T8c	Grainstone-packstone	Os O	Bu Bo	BC
8	T8	T8d	Bioturbated packstone	Os P O Bb	Bu Bo	BC

Biota and allochems (dominant - minor components)

O = oncoids
 BF = benthic foraminifera
 Bb = bivalve bioclasts
 GA = dasycladacean green algae fragments
 Os = ostracods (disarticulated valves)
 G = gastropods (whole shells or fragments)
 L = lithoclasts

Sedimentary - biogenic structures (dominant - minor components)

SL = bed-parallel stromatolitic laminae
 FF = cement-filled fenestral features
 Bu = burrows
 Bo = borings

Diagenetic products (dominant - minor components)

BC = large patches of blocky calcite cement
 GS = geopetal structures